N-δ^{13}C-inclusion profiles of cloudy diamonds from Koffiefontein: evidence for formation by continuous Rayleigh fractionation and multiple fluids

S. Timmerman[a*], A.L. Jaques[a], Y. Weiss[b,c], J.W. Harris[d]

[a] Research School of Earth Sciences, Australian National University, 142 Mills Road, Acton ACT 2601, Australia

[b] Lamont-Doherty Earth Observatory, Columbia University, New York, New York 10964, USA

[c] The Freddy and Nadine Herrmann Institute of Earth Sciences, The Hebrew University of Jerusalem, Jerusalem 91904, Israel

[d] School of Geographical and Earth Sciences, University of Glasgow, Glasgow, G12 8QQ, UK

*corresponding author: suzette.timmerman@anu.edu.au

Abstract

Six diamonds with a fibrous core, intermediate zone and monocrystalline outer zone ('cloudy diamonds') from the Koffiefontein mine, South Africa, were investigated for N concentrations, carbon isotope compositions and micro-inclusion compositions along core to rim traverses. This study evaluates the nature of the change from fibrous to gem diamond growth and the relation between major element composition of high density fluid inclusions and N−δ^{13}C in fibrous growth zones. Three diamonds contain saline to carbonatitic fluid micro-inclusions with constant or increasing carbon isotope values which are inferred to have formed by varying amounts of Rayleigh fractionation in a closed system of a carbonate-bearing fluid. Continuous N−δ^{13}C fractionation trends from the fibrous to gem growth zone in two of the diamonds and equally low nitrogen aggregation states indicate formation of diamond shortly before kimberlite eruption

from a single fluid without a time gap between fibrous and gem diamond growth. High major element/CO_3^{2-} ratios in the growth media resulted in a constant major element composition of the fluid inclusions found in the studied fibrous diamonds. The transition from fibrous to gem diamond growth is likely caused by the precipitation of diamond reducing the degree of oversaturation of carbon in the fluid and hence decreasing the rate of diamond growth. Two other diamonds have inclusions that change from silicate minerals in the inner fibrous growth zones towards pure saline fluid compositions in the outer fibrous growth zones. This decrease in Si, Mg and Ca and increase in K and Cl in the inclusions is accompanied by a decrease in $\delta^{13}C$ values and N contents. These trends are suggested to be the result from gradually mixing in more saline fluids with lower $\delta^{13}C$ values. One diamond with silicic inclusions has significant N aggregation into B-centres, suggesting this fluid is different and that diamond formation occurred significantly (e.g. 1250°C gives ≥10 Ma) before the kimberlite eruption.

Keywords: carbon, diamond, evolution, fluid inclusions, HDF (High Density Fluid)

1. Introduction

'Fibrous' diamonds, including diamonds with cube-like morphology, fibrous coats overgrown on monocrystalline diamond ('coated diamond') and monocrystalline diamonds with internal zones of fibrous growth ('cloudy diamonds'), commonly encapsulate high density fluids (HDFs) as micro-inclusions. These HDFs represent the mediums from which fibrous diamond crystallize, and four compositional HDF end-members have been identified: silicic, saline, low-Mg carbonatitic, high-Mg carbonatitic (e.g., Klein-BenDavid et al., 2004; Klein-BenDavid et al., 2009; Navon et al., 1988; Smith et al., 2012; Tomlinson et al., 2006). The hydrous silicic end-member is rich in SiO_2, Al_2O_3, K_2O and water, whereas the saline end-member has high concentrations of water, K_2O, Na_2O, and Cl, and low contents of MgO, SiO_2, and Al_2O_3. Both carbonatitic HDFs are rich in carbonate, CaO, FeO, and MgO (with the high-Mg carbonatitic end-member typically having MgO>20 wt%, compared to MgO≈10% in low-Mg carbonatitic compositions), and low in SiO_2, Al_2O_3 and water. HDFs of similar compositions have recently been found in several

monocrystalline diamonds as well, as micro-inclusions in octahedral diamonds (Weiss et al., 2014), in twinned crystals (macles) along the twinning plane (Jablon and Navon, 2016), and as thin films (≤ 1.5 μm) around typical mineral inclusions in gem-quality diamonds (Nimis et al., 2016). These findings suggest that the different types of HDFs found in fibrous diamonds are also important in forming monocrystalline gem-quality diamonds (Jablon and Navon, 2016).

The composition of the HDFs varies along two continuous arrays, between the silicic to low-Mg carbonatitic end-members and between the saline to high-Mg carbonatitic end-members (Weiss et al., 2009 and references therein). These variations suggest a possible genetic relationship and evolution between different HDF end-members, and different models have been proposed for explaining the observed compositional trends. Schrauder and Navon (1994) considered melting of carbonated peridotite and eclogite followed by crystallisation of carbonate to explain the silicic to low-Mg carbonatitic trend. Mixing between HDFs of different compositions was suggested by Safonov et al. (2007) and Zedgenizov et al. (2009), while fractional crystallization of carbonates and liquid immiscibility from a parental carbonatitic end-member was proposed by Klein-BenDavid et al. (2007) to explain the two compositional arrays. Based on the similarity to near-solidus melts of eclogite and peridotite in the presence of carbonate and water (Brey et al., 2008; Kessel et al., 2005; Yaxley and Brey, 2004), Weiss et al. (2011); Weiss et al. (2009) suggested that the silicic to low-Mg carbonatitic HDFs are related to melts of hydrous eclogite (±carbonate), whereas the high-Mg carbonatitic HDFs originate from melts of carbonated peridotite. The saline fluids were suggested to be derived from subducted slabs (Weiss et al., 2015) based on positive Sr and Eu anomalies and radiogenic strontium ratios of saline HDFs in a suite of fibrous diamonds from the Ekati and Diavik mines in the central Slave Craton. They further proposed that saline fluids evolve to both silicic and carbonatitic HDFs by subsequent fluid-rock interaction and melting in eclogite and peridotite lithologies, respectively. The recent literature thus shows that it is still unclear what constitutes the parental diamond-forming fluids, how these fluids evolve, whether the mechanisms for formation of fibrous and

monocrystalline diamonds are identical, and if there are any systematic variations between HDFs-bearing diamonds from different kimberlites and cratons.

Individual kimberlites (and kimberlite clusters) tend to carry fibrous diamonds with a predominant HDF type (e.g., Izraeli et al., 2001; Izraeli et al., 2004; Klein-BenDavid et al., 2009; Schrauder and Navon, 1994; Tomlinson et al., 2006), similar to the case for mineral inclusions in monocrystalline diamonds which commonly have a predominant peridotitic or eclogitic paragenesis (Stachel and Harris, 2008 and references therein). Differences in HDF composition, however, between diamonds from a single kimberlite pipe do occur and compositional variations and evolution trends within individual diamonds have been reported (Klein-BenDavid et al., 2004; Shiryaev et al., 2005; Weiss et al., 2009). Therefore, it is important to investigate the compositional change from core-to-rim in HDF micro-inclusions-bearing diamonds to better define the evolution paths of diamond-forming media.

Here we report and investigate the relationships between micro-inclusion major-element compositions, the carbon isotopic compositions, and the nitrogen (N) concentrations and aggregation state along core-to-rim traverses in six cloudy diamonds from the Koffiefontein mine in South Africa. Based on these, we investigate the possible processes (mixing, fractional crystallisation, new fluid) responsible for the evolution of diamond-forming media in both micro-inclusions-bearing fibrous/polycrystalline and monocrystalline diamond growth habits of the studied diamonds.

2. Geological background

The Koffiefontein kimberlite is located at the southwestern region of the Kaapvaal Craton and was emplaced at 90.4 Ma (Davis, 1978; Rickard et al., 1989). Inclusions in diamonds from the Koffiefontein mine are predominantly of the peridotitic suite (81% P-type and 19% E-type based on silicate inclusions

abundances; Harris and Gurney, 1979; Rickard et al., 1989). The peridotitic diamonds have a lithospheric origin. Geothermobarometry calculations of their mineral inclusions indicate diamond formation between 4.5-5.7 GPa and 940-1180°C (Rickard et al., 1989), except for several diamonds with ferro-periclase inclusions that are considered to originate from higher pressure and temperature conditions (i.e. the lower mantle; Deines et al., 1991; Rickard et al., 1989; Smith et al., 1984). Diamond formation ages were inferred from dating inclusions in monocrystalline diamonds. Re-Os dating of sulphide inclusions in a single peridotitic diamond gave an age of 69±30 Ma (Pearson et al., 1998), within error of the age of the kimberlite (Rickard et al., 1989). Sulphide inclusions in several eclogitic diamonds from Koffiefontein yielded much older Re-Os ages, ranging from 1.1 to 2.9 Ga (Pearson et al., 1998).

Fibrous diamonds are common amongst diamonds from Koffiefontein, making up to 28% of the mine retrieval (Rickard et al., 1989). They contain saline HDF micro-inclusions, as well as mineral micro-inclusions of both peridotitic and eclogitic paragenesis (Izraeli et al., 2001; Izraeli et al., 2004). The mineral micro-inclusions record P-T conditions of 4-6 GPa and 1000-1200°C (Izraeli et al., 2004), similar to the conditions recorded by large mineral inclusions in monocrystalline Koffiefontein diamonds (Rickard et al., 1989). The lower N aggregation state of the fibrous diamonds (Type IaA ; N aggregated as pairs in A-centres; 100% A; Izraeli et al., 2001; Izraeli et al., 2004) compared to monocrystalline diamonds (Type IaAB; N aggregated as pairs in A-centres and as four N atoms around a vacancy in B-centres; between 0 and 100% B; Deines et al., 1991; Pearson et al., 1998) from Koffiefontein can be explained by lower mantle residence temperatures or a shorter mantle residence time (Boyd et al., 1987; Navon, 1999).

3. Methods

A suite of six cloudy diamonds from the Koffiefontein mine, South Africa (Fig. 1), weighing between 8.4-15.4 mg, were investigated in the present study (Fig. 1). The samples were first polished into plates along the [100] plane for cubic and [110] for dodecahedral morphologies, respectively. They were then cleaned

with ethanol prior to mounting in indium and gold coating for CL imaging and SHRIMP analysis. Subsequently, the gold coating was removed and the diamonds plates were re-coated with carbon for SEM-EDS analysis. The coating was then removed, and the diamond plates were extracted from the indium mounts for FTIR analyses.

3.1.1. Fourier Transform Infra-Red (FTIR)

Infrared absorption spectra were collected on a Hyperion2000 microscope attached to a Bruker A-670 Hyperion FT-IR spectrometer equipped with a KBr beam splitter, a 15x condenser lens, and a liquid N_2 cooled MCT detector at the Research School of Earth Sciences (RSES), the Australian National University (ANU). All spectra were collected in transmission mode with an aperture size of 100×100 µm, between 4000 to 400 cm^{-1} with a resolution of 4 cm^{-1}. After baseline correction and normalizing the spectra to a 1 cm diamond thickness with an absorption coefficient of 11.94 at 1995 cm^{-1} (Mendelssohn and Milledge, 1995), the N concentration and aggregation states were calculated using an Excel spreadsheet (cabxd97n) provided by D. Fisher (DeBeers Technologies UK). FTIR spectra also record the presence of minerals, fluids and/or volatiles within the micro-inclusions. Following Weiss et al. (2010), the $H_2O/(CO_2+H_2O)$ ratios of the trapped HDFs were calculated with the absorption coefficients of calcite (739 at 1430 cm^{-1}) and water (87 at 3420 cm^{-1}) .

3.2.1 Cathodoluminescence imaging and SEM-EDS analyses

Black and white cathodoluminescence (CL) imaging of the diamond plates were collected at 15 kV on a JEOL JSM-6610A analytical Scanning Electron Microscope equipped with a Robinson CL Detector at RSES.

Individual micro-inclusions were measured using a Hitachi 4300 FE/SEM equipped with an 80 mm^2 X-ray energy dispersive spectrometer (EDS) at the Centre for Advanced Microscopy CT lab of the Australian Microscopy and Microanalysis Research Facility at ANU. Backscatter electron imaging (BSE) was used to

identify micro-inclusions, while secondary electron imaging (SEI) was used to exclude exposed inclusions. Each inclusion was analysed for 60 seconds using an acceleration voltage of 15 kV and a beam current of 1.3 ηA. The data were reduced with a ZAF correction to yield abundances of Na, K, Al, Si, Mg, Ca, Fe, Ti, P, and Cl. Barium and Cr were also analysed; however, Ba was not present in quantifiable amounts and Cr was below detection limit. The analyses were calibrated with the mineral standards: albite (Na, Al), sanidine (K, Si), diopside (Ca), LaP_5O_{14} (P), periclase MgO (Mg), hematite Fe_2O_3 (Fe), rutile TiO_2 (Ti), barite $BaSO_4$ (Ba) and NaCl (Cl). The low totals of the analyses (10.7±4.6 wt %) reflect the small size of the inclusions (0.1-1 μm), their high water and carbonate contents, and their depth below the diamond surface. Therefore, oxide contents were normalized to 100% on a carbon- and water-free basis in order to compare different analyses.

3.2.2 SHRIMP-SI

Carbon isotope measurements along core-to-rim cross-sections were carried out on the SHRIMP-SI at RSES. During pre-sputtering of a spot, the background signal was measured 6 times for 20 seconds. This was followed by optimizing the beam through horizontal and vertical steering and centering. Subsequently data were collected in 6 scans of 20 seconds each. The spot size was ~27 μm in diameter. Analyses were performed with a 15 keV $^{133}Cs^+$ primary beam with a current of 13 ηA. The mass resolution ($m/\Delta m$) of >5000 allowed the separation of $^{13}C^-$ and $^{12}CH^-$ ions. $\delta^{13}C$ values were calculated relative to diamond standard MC08 (-8.85‰ vs PDB; Stern, 2014) that had a precision of 0.27‰ 2SD (n=57). An in-house synthetic diamond standard (BS249=-24.9‰; synthesized by converting graphite into nano-polycrystalline diamond under high pressure at the Geodynamic Research Centre at Ehime University; Irifune et al., 2003; and calibrated against the MC08 by SHRIMP analyses) was measured as unknown to check the stability of the SHRIMP during analyses and yielded a value of $\delta^{13}C$=-24.87 ± 0.30‰ (n=61).

4. Results

4.1 Diamond samples

Cathodoluminescence (CL) images of the diamonds show bright white CL intensities for the monocrystalline inner most core and/or the outer growth zones in the different diamonds, while the fibrous and/or polycrystalline inner and intermediate growth zones have typically lower luminescence and appear dark grey (Fig. 1). Exceptions are the dark grey CL intensity with bright lines of the outer monocrystalline zones of diamond 21 and 23 (Fig. 1b and c), which are potentially caused by low N concentration and the presence of internal stress and associated defects (Goss et al., 2003; Harte et al., 1999). The overall trend of the diamonds from fibrous to monocrystalline growth indicates a decreasing growth rate outwards (Tappert and Tappert, 2011 and references therein).

Detailed descriptions of the growth pattern, carbon isotopic composition, and N concentrations and aggregation in each diamond sample is provided below. The micro-inclusion compositions are described as well. Figure 2 presents the different compositions projected onto a Si+Al-Ca+Mg+Fe-K+Na ternary diagram, in comparison to HDF compositions of previously studied diamonds (Izraeli et al., 2001; Klein-BenDavid et al., 2009; Kopylova et al., 2010; Navon et al., 1988; Schrauder and Navon, 1994; Tomlinson et al., 2006; Zedgenizov et al., 2009). Diamonds 21, 23, and 28 have a range of HDF compositions that are intermediate between the saline and carbonatitic compositions (Fig. 2). Diamonds 20, 27 and 29 are characterized by micro-inclusions in the innermost fibrous core/intermediate layer that contain a mixture of minerals (clinopyroxene, talc, quartz) and saline or silicic HDFs.

Diamond 20

The diamond has a resorbed cubic fibrous core, a resorbed cubic intermediate zone, and a monocrystalline outer zone (Fig. 1a). The core has a $\delta^{13}C$ composition ranging from -4.5 to -4.7‰, followed by a decrease in the intermediate zone to -5.2‰, with a further decrease to -6.2‰ in the outer monocrystalline zone (Table

1; Fig. 3a). The N content decreases simultaneously from 687 ppm to 371 ppm in the core and then increases in the intermediate zone (545 ppm) to 758 ppm in the most outer zone (Table 1; Fig. 3a). The N aggregation is 100% A-centres throughout the diamond (Supplementary information Figure A1). The proportions of clinopyroxene *vs.* HDF within micro-inclusions in this diamond decrease gradually from the centre outwards, as evident by the decrease in silica content from 58 to 18 wt% (Table 2; Fig. 3a). This is accompanied by decreases in MgO (15 to 8 wt%) and CaO (18 to 8 wt%) and a marked increase in K_2O (0 to 26 wt%) and Cl (0 to 9 wt%; Supplementary information Table 1). MgO, CaO are positively correlated with SiO_2, and Cl is positively correlated with K_2O, whereas MgO, CaO, and SiO_2 correlate negatively with Cl and K_2O.

Diamond 21

The diamond consists of a cubic fibrous core surrounded by a fibrous intermediate zone and a monocrystalline outer zone (Fig. 1b). The $\delta^{13}C$ values are constant in the fibrous core (-5.6 to -5.8‰), whereas in the two intermediate zones and single outer zone the compositions increases gradually to -2.8‰ (Table 1; Fig. 3b). This increase in $\delta^{13}C$ is accompanied by decreasing N concentrations from 273 ppm in the core to 99 ppm in the rim. The N aggregation state is 100% A-centres throughout the diamond. The average fluid micro-inclusion compositions in the core and intermediate growth zone are within error (Table 2; Fig. 3b) and have a carbonatitic-saline composition with 6-17 wt% MgO, 3-29 wt% CaO, and 12-32 wt% Cl (Supplementary information Table A1). The variable presence of carbonates in inclusions likely caused the variation between individual analyses.

Diamond 23

This diamond is characterised by a fibrous core surrounded by a polycrystalline intermediate zone and a monocrystalline outer zone (Fig. 1c). This diamond has a clear trend of continuously increasing $\delta^{13}C$ values and decreasing N concentrations from core to rim (Fig. 3c). The carbon isotope value increases from -6.2‰ to -4.9‰, whereas the N content decreases from 755 to 105 ppm (Table 1). The N aggregation state is 100%

A-centres throughout the diamond. Despite significant changes in N content and $\delta^{13}C$ in the core and intermediate zone, the average micro-inclusion compositions remain similar (Table 2; Fig. 3c). The inclusions have an HDF composition near the saline end-member, with low SiO_2 (<6 wt%), high Cl (21-42 wt%), and relatively low CaO (3-14 wt%; Supplementary information Table A1).

Diamond 27

This diamond has a polycrystalline inner and outer core, a fibrous intermediate zone and a monocrystalline outer zone (Fig. 1d). The outer growth layers are characterised by octahedral growth. The inner core has a $\delta^{13}C$ value of -5.9‰, increases to -5.1‰ in the outer core before steadily decreasing to the intermediate/rim boundary where the value is -5.8‰ (Fig. 3d). This is followed by a sharp rise to -4.9‰ and to -4.2‰ in the monocrystalline outer zone. The N concentration decreases from 835 to 463 ppm from the cores to the intermediate zone, and then sharply increases to higher N concentrations (724 ppm) at the start of the rim, falling steadily to 517 ppm at the diamond edge. There is a significant change in the N aggregation state, from 27% B-centres in the core to 13% in the rim (Table 1). The average fluid micro-inclusion composition has a small change from core to the intermediate zone from 58 to 53 wt% SiO_2, from 11 to 16 wt% K_2O, and from 9 to 6 wt% MgO (Table 2).

Diamond 28

The diamond has a monocrystalline core, a fibrous intermediate zone and a monocrystalline outer zone. The core and intermediate fibrous growth zone of this diamond are characterized by limited change in carbon isotope composition between -4.7 and -5.5‰ and in N concentrations of 946 to 1066 ppm. A sharp change is observed for the monocrystalline outer zone, which has a lower $\delta^{13}C$ composition (-6.5 to -6.8‰) and decreasing N concentrations from 836 to 565 ppm (Table 1; Fig. 3e). The monocrystalline core has an aggregation state of 4% B-centres, followed by 1.3-1.9% B-centres in the fibrous zone and no B-centres present in the outer zone (Table 1). The fluid micro-inclusion compositions remain relatively constant in

the fibrous intermediate growth zone with saline compositions (5±2 wt% SiO_2, 35±3 wt% Cl, 32±4 wt% K_2O; errors 1SD; Table 2).

Diamond 29

Diamond 29 has a cubic monocrystalline core, a fibrous intermediate zone and a monocrystalline outer zone, characterized by a cubic morphology (Fig. 1f). The monocrystalline core of this diamond has a $\delta^{13}C$ of -3.6 to -3.7‰. The fibrous intermediate growth zone shows a small change in $\delta^{13}C$ from -3.0 to -3.6‰, with N contents changing from 1334 to 1096 ppm. The monocrystalline outer zone is characterised by a sharp change in $\delta^{13}C$ values (-5.8 to -5.2‰) which is accompanied by a drop in N concentrations to 317 ppm at the diamond rim (Fig. 3f). The monocrystalline core has significant N aggregation with 14-21% B-centres. Along the traverse, the FTIR spot analyses of the intermediate fibrous growth zone directly around the monocrystalline core showed 0% B-centres on one side and 15.7-19.6% B-centres on the other side. Given the thickness of the plate and the size of the spot analyses (100x100 μm), the N discrepancy is likely caused by overlapping of the core and intermediate zone on one side. The micro-inclusions show major changes from silica-rich towards saline compositions within the fibrous intermediate growth zone; from 54-58 wt% to 0-14 wt% SiO_2, <2 wt% to 24-40 wt% K_2O, and <0.8 wt% to 29-45 wt% Cl. A positive correlation exists between SiO_2, MgO, and CaO, and between Cl and K_2O, whereas SiO_2, MgO, and CaO are negatively correlated with Cl and K_2O.

4.2 Diamond impurities - FTIR spectroscopy

All the diamonds contain carbonate- and water-bearing micro-inclusions as evidenced by the IR absorption peaks at ~880 and 1450 cm^{-1} for carbonate, and ~1650 and 3000-3600 cm^{-1} for water and OH stretching (Fig. 3 and Supplementary information Fig. A2). The $H_2O/(H_2O+CO_2)$ ratio of the bulk fluid estimated by the relative absorbance of H_2O and carbonate peaks indicate that the fluids are strongly hydrous with $H_2O/(H_2O+CO_2)$ ratios of 0.49-0.92. In most cases, the innermost fibrous growth zones have stronger H_2O

IR absorption at 3000-3600 cm^{-1} than subsequent growth zones that contain micro-inclusions in the same diamond (Supplementary information Fig. A2), which likely relates to decreasing inclusion density outwards. Mineral absorption peaks are also observed (Fig. 4), and the different phases were identified based on the IR-mineral database of rruff.info. The core of diamond 20 shows peaks at 923 and 972 (clinopyroxene (cpx)/garnet (grt)), and 1075 cm^{-1} (cpx). The outer zone of this diamond shows peaks at 700 (cpx), 882 (grt), 905 (grt), 972 (cpx/grt), 1077 cm^{-1} (cpx), and 765 associated with silicates, similar to the core. IR peaks in the core of diamond 21 are at 718 (calcite) and 960 cm^{-1} (grt). The intermediate zone of this diamond shows a peak at 954 cm^{-1} (silicates). In the core and intermediate zone of diamond 23 a strong peak at 3690 cm^{-1} and 950-1000 cm^{-1} is due to the presence of mica. Additional silicate peaks are present at 905 (grt), 932 and 972 (cpx/grt), and 1082 cm^{-1} (cpx). Diamond 27 shows peaks at 685 (possibly talc), 782 and 804 (quartz), 1003-1013 (phlogopite or talc), and 1088 cm^{-1} (quartz). Diamond 28 shows silicate peaks at 727, 878, ~977 (grt/cpx), and 1002 cm^{-1} (mica). Diamond 29 shows peaks at 876, 900, 974 and 1001 cm^{-1}, similar to diamond 28.

4.3 Mineral micro-inclusions

In total 26 mineral micro-inclusions (<2 μm) were analysed by SEM-EDS (Table 3). The corrected compositions of clinopyroxene inclusions of diamond 20 and 29 that had a small fraction of fluid are included in Figure 5. Calcite was found in diamonds 20 and 27, and Ca-Mg-Fe carbonates with up to 20 mol% Fe (dolomite) in diamond 21. These inclusions are similar in composition to carbonate micro-inclusions found in previously studied Koffiefontein fibrous diamonds of both the eclogitic and peridotitic paragenesis (Izraeli et al., 2004). Diamond 20 contains also pyrope-almandine garnet micro-inclusions and omphacitic pyroxene inclusions, indicating an eclogitic origin (Fig. 5). Both the pyrope-almandine garnet and the omphacite compositions are similar to those previously reported as micro-inclusions in eclogitic fibrous diamonds from Koffiefontein (Izraeli et al., 2004) and large mineral inclusions in monocrystalline diamonds (Meyer, 1987; Stachel and Harris, 2008). While garnet, clinopyroxene and mica peaks are present

in the FTIR spectra, these minerals were not found by SEM in diamond 23 and hence its paragenesis is undetermined. Two SiO_2 (quartz or coesite) inclusions were identified in diamond 27, suggesting an eclogitic origin, as well as one micro-inclusion having the composition of $Mg_{2.36}Fe_{0.18}Al_{0.09}Si_{3.61}O_{10}$ which is similar to talc (Farmer, 1958). Diamond 28 contains orthopyroxene (enstatite-ferrosilite) micro-inclusions. Their compositions are lower in Si, Mg and higher in Fe compared to large peridotitic enstatite inclusions in monocrystalline diamonds in general (e.g., Stachel and Harris, 2008), and to those found previously as micro-inclusions in fibrous diamonds (Izraeli et al., 2004) and as macro-inclusions in monocrystalline diamonds (Rickard et al., 1989) from Koffiefontein. The Si, Mg, Fe contents and Mg# of 75-76 (Mg# = 100×Mg/(Mg+Fe) mole percent) are close in composition to websteritic inclusions, intermediate between the peridotitic and eclogitic paragenesis (Stachel and Harris, 2008). The orthopyroxenes have slightly lower Mg# than the websteritic field defined by Stachel and Harris (2008; Fig. 5). Diamond 29 contains clinopyroxene inclusions with compositions similar to diopside rather than an eclogitic clinopyroxene (Table 5 of Stachel and Harris, 2008), based on the MgO, CaO, and Na_2O contents. These micro-inclusions contain varying amounts of saline HDF, and therefore the analyses were corrected by subtracting the Cl plus the same amount of positive K ions and re-normalising to 100%. The relatively high alumina contents (4.6-7.4 wt%), low Cr (Cr below detection limit) and relatively Fe-rich compositions (Mg# = 82) likely indicate a websteritic paragenesis.

5. Discussion

Three diamonds (21, 23, 28) have a similar range in HDF composition and constant or increasing carbon isotope values in the fibrous growth zone. The other diamonds (20, 27, 29) contain HDFs that show a decrease in the silica content of the micro-inclusions (from silicates to pure fluid) with simultaneously a decreasing carbon isotope value in the fibrous growth zone. The changes observed in the major element composition of micro-inclusions and the carbon isotope values of the latter three Koffiefontein diamonds suggest a genetic relationship between diamond growth and HDF compositions. These changes therefore

can provide new insights in understanding mantle processes involving carbon-bearing fluids and diamond formation. We examine these compositional variations and discuss three different models that could explain the trend in diamond $\delta^{13}C$ and micro-inclusions major element composition: 1) HDF mixing with new infiltrating fluids, 2) fractional crystallisation from an evolving HDF, 3) a mixture of minerals and HDF. Finally, we examine the changes in N aggregation state and N-$\delta^{13}C$ from fibrous to gem diamond growth to assess the potential implications for relative timing of fibrous and monocrystalline diamond growth.

5.1 Variation in HDF and diamond compositions

5.1.1 Constant HDF and diamond carbon isotope composition

Three diamonds (21, 23, 28) with near constant or increasing carbon isotope values within the fibrous growth zones show no change in their saline or carbonatitic HDF micro-inclusion compositions (Fig. 2). Diamond 28 has a constant $\delta^{13}C$ in the fibrous growth zone. A constant carbon isotope composition indicates diamond formation in either an open system or quasi-open system, as Rayleigh fractionation is only detectable in a closed system when more than 5% of the fluid is consumed (Cartigny et al., 2001). In a quasi-open system it is likely that the major element composition of the diamond-forming HDF would also remain constant, and result in similar HDF micro-inclusion compositions throughout the fibrous growth zone, of which diamond 28 is an example. The monocrystalline rim of diamond 28 however has a distinctly different carbon isotope composition and N concentration compared to its core and intermediate zones (Fig. 6), suggesting the monocrystalline outer zone formed by a different fluid.

The monocrystalline rims of diamonds 21 and 23 show a continuation of the overall trends in decreasing N content and increasing $\delta^{13}C$ values in the fibrous intermediate zones (Fig. 3). For diamonds 21 and 23, it seems more likely that the observed increase in carbon isotopic values were caused by Rayleigh fractionation of a single fluid that became less saturated in carbon, leading to slower monocrystalline diamond growth. As mentioned in Shirey et al. (2013 and references therein) a number of previous studies of fibrous diamonds have found a consistent increase of ~3‰ in $\delta^{13}C$ (from $\delta^{13}C$ of -8‰ to -5‰ from core

to rim) which have been attributed to fractionation during precipitation from oxidised carbon-bearing fluids. Increasing carbon isotope values in peridotitic diamonds can also be caused by carbon isotope fractionation during diamond precipitation from a mixed CO_2-CH_4 fluid (Smit et al., 2016; Stachel et al., 2017). Carbonates are present in diamonds 21 and 23 (carbonate absorption in FTIR spectra; Fig. 4) indicating that the HDFs in these diamonds are oxidised, and that the diamond-forming fluids likely had a dominant CO_2 or CO_3^{2-} carbon speciation. As no other minerals were detected by SEM-EDS, the paragenesis is undetermined. The increase in carbon isotope composition from core to rim in diamond 21 and 23 can be modelled by a Rayleigh distillation process from an oxidised fluid (CO_3^{2-} or CO_2). Figure 6 shows the N−$\delta^{13}C$ changes during such a process, following the formula for Rayleigh fractionation from Cartigny et al. (2001). For a fractionation factor (ΔC) of -1.5‰ ($\Delta_{diamond\text{-}CO3}^{2-}$; calculated at 1200°C) (Chacko et al., 1991), the change in carbon isotope value requires 86% of the carbon fluid to be consumed during precipitation in the case of diamond 21 and 64% in the case of diamond 23 (fraction precipitated = 1 – EXP(($\delta^{13}C$- $\delta^{13}C_0$)/ΔC) (for details see section 4.2 of Cartigny et al., 2001). The lack of change in the major element composition of the HDFs and change in $\delta^{13}C$ during precipitation of diamonds 21 and 23 could be explained by high major element/CO_3^{2-} ratios of the diamond-forming media in a closed system. Thus, during diamond precipitation the carbon isotope composition of the diamond changes while the major oxide compositions of the HDF does not, resulting in carbon isotope fractionation and varying diamond $\delta^{13}C$ values while the major element composition of the micro-inclusions remained unchanged. This is supported by the progression from fibrous to monocrystalline growth with a continuous N−$\delta^{13}C$ change, suggesting that there is less carbon oversaturation. The slower growth will result in less fluid captured as inclusions. The decrease in N abundances towards the rim suggest that N behaves as a compatible element (de Vries et al., 2013; Smart et al., 2011; Stachel et al., 2009; Thomassot et al., 2007). The Rayleigh fractionation lines in Fig. 6 were modelled with the formula of Cartigny et al. (2001) and best fits for a fractionating CO_3^2-bearing fluid were obtained with $\delta^{13}C_0$ is -6.0‰, N is 250 ppm, and a K_N value (N partition coefficient) of 1.6 for diamond 21 and $\delta^{13}C_0$ is -6.1‰, N is 940 ppm, and a K_N value of 3.2 for diamond

23. Modelling the change in N content with a CO_2-bearing fluid gives higher K_N values (2.3 and 6.0 respectively for diamond 21 and 23) and less fluid being consumed by precipitation (57 and 35%) with a fractionation factor of -3.5‰ for $\Delta_{diamond\text{-}CO2}$ at ~1200°C (Chacko et al., 1991). Both CO_3^{2-} and CO_2 Rayleigh fractionation models are viable to explain the change in carbon isotopic composition of diamonds 21 and 23.

5.1.2 Changes in HDF and diamond carbon isotope composition

Three diamonds show a change in major element composition from silicate inclusions towards saline HDF inclusions (diamond 20 and 29) and a small decrease in Si (diamond 27). These compositional trends in the fibrous growth zones can be explained by the presence of mineral inclusions (cpx for diamond 20 and 29; SiO_2+talc for diamond 27) in the micro-inclusions which subsequently became richer in saline HDF. This is accompanied by a decreasing carbon isotope value from the start of the fibrous growth zones to the end of those zones (Fig. 3 and 7b). Diamonds 20 and 27 also show a change in $\delta^{13}C$ from one fibrous growth zone to the next fibrous growth zone. Three models are discussed below that could explain both the major element and carbon isotope compositional changes: 1) mixing with new HDFs, 2) fractional crystallisation, 3) a mix of minerals and HDFs.

5.1.2.1 Changing HDF and diamond carbon isotope compositions - introduction of new fluids

Differences in HDF micro-inclusion and carbon isotope compositions in a new growth zone within a diamond are commonly inferred to result by diamond precipitation from a new fluid or by mixing of different diamond-forming fluids. For example, Klein-BenDavid et al. (2004) ascribed a change from saline to carbonatitic HDF micro-inclusions in a diamond from Diavik to an influx of fresh carbonatitic fluid to form the subsequent growth. Marked changes in carbon isotope values in a single diamond have been used in previous studies as evidence for a new growth event from a different fluid (e.g. Boyd et al., 1992; de Vries et al., 2013; Petts et al., 2016; Smart et al., 2011). The N contents and $\delta^{13}C$ compositions of the monocrystalline outer zones of diamonds 20, 27, and 29 are different to those of their fibrous growth zones.

403 This can be explained by an influx of a new fluid, resulting in the observed abrupt changes in N contents
404 and carbon isotope compositions (Fig. 3).

405

406 Formation of the fibrous growth zones is more complicated. Introduction of a saline HDF may explain the
407 trends from initial silicate inclusions to saline-rich HDF inclusions. A trend towards more depleted ^{13}C
408 isotopic compositions could be caused by mixing of a saline HDF with lower carbon isotopic values. This
409 could explain the gradual major element and $\delta^{13}C$ changes in diamonds 20 and 27. However, in diamond
410 29 the change in major element composition occurs within the first 20 μm of the start of the fibrous
411 intermediate growth zone, while the N concentrations and carbon isotopic values decrease marginally over
412 the entire fibrous growth zone (several 100 μm). The change in major element composition over a short
413 distance indicates that a large volume of fluid came in rapidly, resulting in subsequent diamond
414 precipitation with minimal differences in N- $\delta^{13}C$.

415

416 **5.1.2.2 Changing HDF and diamond carbon isotope compositions - Fractional crystallisation**

417 The compositional spectrum of HDF inclusions in fibrous diamond between the silicic and carbonatitic
418 end-members has been proposed to be caused by fractional crystallisation involving precipitation of garnet,
419 clinopyroxene, olivine, carbonate, apatite, rutile and K-bearing phases (Schrauder and Navon, 1994;
420 Shiryaev et al., 2005; Zedgenizov et al., 2009). Progressive crystallisation of silicates can also cause
421 enrichment in alkali elements, driving a fluid from silicic to saline compositions and may potentially explain
422 some of the major element trends and fractionation of carbon isotope composition observed within our
423 diamond samples. A decrease in Mg, Si, Ca and hence an increase in K and Cl could be caused by
424 crystallisation of silicates and carbonates (grt + cpx + calcite for diamond 20; SiO_2 + talc ± Mg-carbonate
425 for diamond 27; cpx + calcite for diamond 29). The direction of the chemical change during crystallisation
426 of these minerals are compatible with the observed changes in major element compositions (Fig. 7a).

Removal of CO_2 can decrease the $\delta^{13}C$ value of the remaining fluid and subsequent precipitated diamond (Cartigny et al., 2001), based on the fractionation factor of 4‰ for $\Delta_{CO2\text{-}C}$ in a basaltic magma at 1200°C (Bottinga, 1969; Javoy et al., 1978). This might explain the observed decrease in $\delta^{13}C$ value in the fibrous growth zones of diamonds 20, 27, and 29. This will result in a residual fluid that is enriched in elements such as K, Na and Cl. Modelling of this process for both the change in SiO_2 content and carbon isotope composition was done with a C fractionation factor of 4‰ ($\Delta_{CO2\text{-}C}$), 40 wt% CO_2 volatiles-60 wt% major oxides (based on Navon et al., 1988), and assuming a loss of 1 mol of SiO_2 for each mol of CO_2. This model seems incapable of explaining the isotopic and compositional changes for diamonds 20, 27, and 29 (Supplementary information Figure A3). If, however, CO_2 was removed with a silicic melt from a C or CO_3^{2-}-bearing fluid, the carbon isotope fractionation is expected to be smaller and the observed SiO_2-$\delta^{13}C$ changes could be explained with a lower ΔC (0.6-3‰) or a higher SiO_2/CO_2 ratio.

5.1.2.3 Changing HDF and diamond carbon isotope compositions - Mix of minerals and fluids

Linear arrays of EPMA analyses of micro-inclusions extending between a mineral composition and the saline HDF composition were described by Izraeli et al. (2004) who interpreted them as mixing of mineral inclusions and varying proportions of HDF. Linear compositional trends found in our three diamonds can similarly be accounted for mixing minerals and HDFs in different amounts (Fig. 7a). The trend of the analysed inclusions in diamond 20 can be explained as mixing between omphacitic clinopyroxene and saline HDF with a composition of $K_{13.25}Fe_{4.29}Mg_{2.64}Ca_{1.58}Si_{0.50}Al_{1.29}O_{23.55}Cl_{5.93}$ (Fig. 7a). The analysed micro-inclusions in the core of diamond 27 could be explained by a mix of silica (presumed to be quartz) and talc minerals (55%) and a silicic HDF (45%), with a shift to a purely silicic fluid in the intermediate zone. Diamond 29 has inclusions that show a decrease in Mg, Ca, Si and an increase in K and Cl. The innermost fibrous growth zone of diamond 29 contains diopside inclusions and the intermediate micro-inclusion compositions can be modelled by a mix of 50-60% diopside and 50-40% saline HDF. The last

stages of fibrous growth trapped micro-inclusions of pure saline HDF composition. In each of these diamonds the mixes between minerals and fluids are not random. There are high percentages of minerals in the inclusions in the inner fibrous growth zone, whereas micro-inclusions in the outer fibrous growth zones are characterised by pure HDF compositions. This suggests that the trends are most likely caused by progressive addition of fresh saline HDF.

The large decrease in SiO_2 contents (in wt%) is accompanied by a small decrease in N content (by 100−300 ppm) and decrease in $\delta^{13}C$ values (by 0.4−1.1‰). Carbon isotope fractionation occurs during Rayleigh fractionation from different carbon speciations (CH_4, CO_2, CO_3^{2-}) (Chacko et al., 1991; Richet et al., 1977) and by removal of CO_2 or carbonates with heavier $\delta^{13}C$. Recently it has been suggested that diamonds can be formed from organic carbon species during a pH drop and that a change in the pH can cause a change in the $\delta^{13}C$ value (Sverjensky and Huang, 2015). While there are no studies on the influence of the non-carbon-bearing major element composition of the fluid on carbon isotope fractionation, previous studies have shown the effects of temperature, pressure and solute composition of the fluid on hydrogen isotope fractionation (Chacko et al., 2001 and references therein). Sverjensky and Huang (2015) also proposed that the formation of diamond is a result of changes in the aqueous fluid chemistry related to silicate minerals. The reaction of silicates with hydrogen and, subsequently, hydrogen with aqueous organic carbon species in the diamond-forming media, suggest silicates could have an indirect influence on the carbon isotope composition. This study shows that the slopes of the decrease in silica and $\delta^{13}C$ for diamonds 20 and 29 are reasonably similar and range from 0.009 to 0.014 $\Delta\delta^{13}C/\Delta Si$ (Fig. 7b), supporting a possible influence. However, it is important to note that the $\delta^{13}C$ range in fibrous diamonds is small (-3 to -8‰; Boyd et al., 1987), suggesting any potential influence of the fluid major element composition on carbon isotope fractionation will be limited.

While it is likely that minerals other than diamond crystallise from a diamond-forming fluid, decreasing the amount of silica from 60 wt% to about 5 wt% (diamond 29) to drive the HDF composition from silica-rich

to saline by fractional crystallisation of silicates alone is, however, very difficult and would require crystallisation of most of the SiO_2 of the initial fluid. The discrepancy between the change in HDF major element composition, N contents, and $\delta^{13}C$ in a fractional crystallisation model suggest this process did not play a significant role in diamond 20, 27, and 29. Mixes between minerals and an incoming HDF is therefore the most reasonable model to explain the large decrease in silica and presence of the purest mineral micro-inclusions at the inner most part of the fibrous growth zone. This can also explain why some inclusion compositions of diamond 20 and 29 traverse the gap between the major carbonatite−silicic and carbonatite−saline trends exhibited by HDFs in the present fibrous diamonds (Fig. 2 and 7a).

5.2 Origin of the mineral inclusions

The presence of pure mineral micro-inclusions in fibrous diamonds has lead to the interpretation of the mineral micro-inclusions being remnants of the lithospheric host rock, in which the diamond grew during HDF percolation (e.g., Izraeli et al., 2004; Logvinova et al., 2008; Tomlinson et al., 2006). This is supported by the similarity of the Mg# and composition of peridotitic mineral micro-inclusions in Koffiefontein diamonds to the large mineral inclusions found in diamonds from that mine, but also to those in peridotitic diamonds worldwide (Izraeli et al., 2004; Meyer, 1987). In this scenario the mineral micro-inclusions are closely related to the diamond lithospheric host rock, as remnants of the growth environment (Logvinova et al., 2008; Nestola et al., 2014).

In our study, the sub-micron spherical mineral inclusions (SiO_2, talc, orthopyroxene, clinopyroxene, garnet) are of the eclogitic and websteritic parageneses. Our pyroxene and garnet mineral inclusions generally fall just within the wide range in eclogitic and websteritic compositions defined by larger mineral inclusions in monocrystalline diamonds (Stachel and Harris, 2008), with the orthopyroxene of diamond 28 having slightly lower Mg# than the defined range (Fig. 5). This indicates that the orthopyroxenes are remnants of lithospheric host rock of unusual iron-rich composition, modified by metasomatic fluids and thus syngenetic. An alternative possibility is that some of the mineral inclusions crystallised directly from the

HDF during cooling. Kopylova et al. (2010) suggested that amorphous Na-Mg-Ca-Fe carbonates (determined by FTIR-Raman-XRD), along with high-Si mica and apatite, were precipitates from carbonatitic-silicic fluid inclusions trapped in Congo diamonds. Clinopyroxenes with high K_2O (1 wt%) have been suggested to grow in K-rich environments, reflecting interaction with metasomatic fluids (Harlow, 1997; Izraeli et al., 2001). Experiments on interaction of silicic fluids with peridotite (Rapp et al., 2017) and crystallisation of high-Si mica, carbonate and apatite in a closed system (Kopylova et al., 2010) suggest it is possible to drive the HDF from silicic to residual saline compositions. However, a syngenetic origin of most silicate minerals in fibrous diamonds is generally thought to be unlikely due to the low Si-content of the trapped HDF inclusions (e.g, Tomlinson et al., 2006), especially those rich in carbonate, KCl and H_2O (saline to carbonatitic HDFs). The Mg# of the melt in diamond 20 (55-72) is likely in equilibrium with the garnet (Mg# 55-57) and clinopyroxene (Mg# 78-84) inclusions, as it is similar to experimental results of a hydrous fluid (Mg# 53-64) at 1100°C and 6 GPa in equilibrium with crystallised garnet (Mg# 55) and clinopyroxene (Mg# 84) (Kessel et al., 2004). Garnet and clinopyroxene can be in equilibrium with a melt of lower Mg# (35-37) when the melt is anhydrous (Spandler et al., 2007). Diamond 23 may be an example of this with Mg# of 31-36 and lower H_2O/CO_2 ratios of 0.49-0.62. Based on the above arguments it remains difficult to establish whether the minerals have crystallised from or are in equilibrium with the diamond-forming fluids which substantially interacted with the mantle host rock, or are direct remnants of the original mantle host rock.

5.3 Timing of fibrous and monocrystalline diamond formation

It is generally assumed that fibrous diamonds formed shortly before eruption of their kimberlite host based on their low aggregation state (Boyd et al., 1987; Navon, 1999). Three of the studied Koffiefontein diamonds (20, 21, and 23) have 100% A-centres, whereas the fibrous and monocrystalline growth zones of diamond 27 (11-27% B-centres) and the monocrystalline core of diamond 28 and 29 (4% and 21% B-centres respectively) have N in B-centres (Fig. 8 and Supplementary information Fig. A1). The aggregation of single N atoms in C-centres to pairs of N in A-centres and conversion of A-centres to four N atoms

around a vacancy in B-centres is strongly influenced by the diamond 'mantle residence temperature', time, and the diamond N concentration (Taylor et al., 1996). The presence of N in pairs (Type IaA diamond) indicates that the Koffiefontein diamonds of this study are relatively young with a short mantle residence time at ambient mantle temperatures (Navon, 1999; Taylor et al., 1996). Pearson et al. (1998) showed that a diamond with 100% A-centres (diamond K306 from Koffiefontein) has a Re-Os age similar to the kimberlite eruption age. Mantle residence times were calculated with the N concentrations and aggregation states of the studied samples at 1050 and 1200°C, which essentially brackets the previously established temperature range (1000-1185°C ± 140°C) for fibrous diamonds from Koffiefontein (Izraeli et al., 2004). As 100% A or 0% B cannot be used in the time and temperature calculations, for calculation purposes 0.001% B-centres was substituted for samples with 0% B-centres. Taylor et al. (1990) noted that at temperatures < 1050°C there is no significant conversion of A-centres to B-centres, even for mantle residence times of several billion years. For the diamonds with ~0% B-centres in this study, the maximum mantle residence time is < 5 Ma at 1050°C. At 1200°C, the highest aggregation state of 27% B-centres for diamond 27 gives a mantle residence time of 56 Ma. The mantle residence times are illustrated in Figure 8 for a temperature of 1150°C. The low aggregation state of both eclogitic and peridotitic fibrous diamonds from Koffiefontein indicates they must have resided at low temperatures and/or formed shortly before kimberlite eruption (Izraeli et al., 2004). The low aggregation state of most of the monocrystalline gem-quality rims surrounding the fibrous layers indicates a similarly young formation age. This would be the case for the studied diamonds 20, 21, 23, 28 and 29.

Older fibrous diamonds may exist, based on the presence of B-centres in cloudy diamonds from Siberia and in a fibrous diamond from Finsch, Kaapvaal Craton (Logvinova et al., 2011; Skuzovatov et al., 2011; Weiss et al., 2014; Zedgenizov et al., 2006). Diamond 27 with higher aggregation states (up to 27% B) may be another such case, and has an age of 280-310 Ma in the core and 118-153 Ma in the outer zone based on its N systematics and a presumed temperature of 1150°C based on the diamond formation temperatures at Koffiefontein (1120±95°C; Izraeli et al., 2004; Rickard et al., 1989). This diamond differs from the other

556 Koffiefontein diamonds from this study as it is the only diamond with silicic HDF inclusions. Previous
557 studies of 55 cloudy diamonds from Siberia with B-centres contained high-Mg carbonates-silicates and Cl
558 present in the fluid phase (up to 20% B, n=20; Logvinova et al., 2011), carbonatitic (15-25% B, n=19;
559 Skuzovatov et al., 2011), and carbonatitic-silicic inclusions (22-67% B, n=16; Zedgenizov et al., 2006).
560 Three saline HDF-bearing diamonds with a small amount of N in B-centres have been reported (2% B-
561 centres in the fibrous growth zone of diamond 28 in this study; 5-6.7% B-centres in two monocrystalline
562 diamonds; Weiss et al., 2014). This indicates silicic-carbonatitic fluids may have been more commonly
563 actively precipitating diamonds longer before kimberlite eruption or at higher temperatures than saline
564 fluids. Further studies are needed to investigate this.
565
566 As both the fibrous and monocrystalline outer growth zones in diamonds 20, 21, and 23 are all 100% IaA
567 diamonds, the time difference between formation of all these different growth zones must have been
568 relatively small; no more than a couple of hundred thousand years (Navon, 1999; Taylor et al., 1996; Taylor
569 et al., 1990). For diamond 27 and 28 differences in N contents, N aggregation state, and $\delta^{13}C$ compositions
570 (Table 1) between the fibrous and monocrystalline growth zones suggests there is a difference in time and/or
571 temperature between their formations. A difference in time is most plausible given the resorption at the
572 intermediate-rim boundary.
573
574 **5.4 Implications for diamond formation**

575 The presence of carbonates and the trends of increasing $\delta^{13}C$ values with decreasing N content in the cloudy
576 Koffiefontein diamonds 21 and 23 of this study indicates formation from oxidised fluids, in agreement with
577 previous studies (e.g. Boyd et al., 1992; Boyd et al., 1994; Klein-BenDavid et al., 2007). So far no evidence
578 for fibrous diamond growth from reduced fluids (e.g. pure CH_4 carbon speciation) has been found. The
579 explanation of the change from silicate minerals to pure fluids (saline for diamond 20 and 29; silicic for
580 diamond 27) caused by introduction of HDF is applicable to other localities. Sudden changes in fluid

581 composition have been suggested to be the result of a new fluid (Klein-BenDavid et al., 2004), and bands
582 with single silicate micro-inclusions found in a cloudy Koffiefontein diamond (Izraeli et al., 2004) were
583 inferred to be the remnants of previous mineral grain boundaries in the mantle. The clinopyroxene micro-
584 inclusions present at the inner most fibrous growth zone in diamonds 20 and 29 of this study are also likely
585 to be (metasomatised) remnants of the host rock. This interpretation is consistent with the model of
586 Sverjensky and Huang (2015) that predicts the breakdown of reactant silicate minerals in the beginning of
587 the reaction progress when a fluid reacts with metasedimentary eclogite to form diamond and carbonates
588 by a drop in pH. While their model is for a carbonatitic fluid, such a process could also potentially be
589 occurring for interaction with saline HDFs.

590

591 Previously it was suggested that the cloudy diamonds at Koffiefontein were formed in one significant event,
592 as the clouds in eclogitic and peridotitic diamonds have similar characteristics (Izraeli et al., 2004) and
593 about 20% of the diamonds recovered at the Koffiefontein mine are cloudy diamonds (Rickard et al., 1989).
594 The cloudy diamonds in this study with saline HDF inclusions in eclogitic and websteritic diamonds have
595 similar characteristics (HDF composition, N content and aggregation) to the previous studied cloudy
596 Koffiefontein diamonds. This indicates that the diamond-forming event was widespread and the saline HDF
597 interacted with peridotitic (Izraeli et al., 2004), eclogitic, and also the more uncommon websteritic
598 lithology. This study and previous studies (Izraeli et al., 2001; Izraeli et al., 2004; Tomlinson et al., 2006)
599 have found saline HDFs in diamonds with eclogitic and now also websteritic inclusions, showing the fluids
600 are not directly associated with a single host rock. The origin of the HDF that formed the young cloudy
601 diamonds with saline HDFs (diamond 20, 21, 23, 28, 29) is undetermined. Saline HDFs have been inferred
602 to be related to subduction of hydrated oceanic crust, based on their high Cl and low K/Cl ratios, trace
603 element patterns and Sr isotopic composition, and the extensive amount of fluid required to be
604 released/formed in a short time period (e.g. Izraeli et al., 2001; Weiss et al., 2015). However, we are not
605 aware of evidence of subduction beneath the Kaapvaal Craton in the late Cretaceous (although earlier

606 subduction has been proposed) and suggest that alternative models for formation of the saline fluids need
607 to be considered. Other possible sources of the saline HDFs might be widespread mantle metasomatism
608 related to proto-kimberlites immediately prior to kimberlite eruption. Further, despite the significance of
609 the diamond-forming event at Koffiefontein not all cloudy diamonds in Koffiefontein were formed in a
610 single event, as the cloudy diamond 27 with silicic HDFs and 27% B-centres was likely formed significantly
611 before kimberlite eruption.

612

613

614 **6. Conclusions**

615 The nature of the change from fibrous to gem diamond growth and the relation between major element
616 composition of micro-inclusions and N−δ^{13}C was investigated in this study for six cloudy Koffiefontein
617 diamonds.

618 1. The studied diamonds from Koffiefontein have eclogitic (diamond 20, 27, and possibly 21, 23
619 based on the presence of mica), and websteritic (diamond 28, 29) parageneses based on analysed
620 micro-minerals.
621 2. The association of saline HDFs with eclogitic and websteritic mineral inclusions in the
622 Koffiefontein diamonds of this study, suggests saline HDFs are pervasive and not only
623 metasomatise eclogitic and peridotitic lithologies in the mantle, but also the more uncommon
624 websteritic lithology.
625 3. Three diamonds (21, 23, 28) have carbonatitic−saline fluid inclusion compositions with constant
626 or increasing carbon isotope compositions in their fibrous growth zones, and formed from oxidising
627 fluids with various amounts of Rayleigh fractionation. Two diamonds (20, 29) show internal
628 changes from silicate minerals to saline fluid compositions between and within single growth zones
629 that are coupled with a simultaneous small decrease in carbon isotope composition and N content.
630 These diamonds formed by mixing of silicates with a depleted ^{13}C saline fluid.

4. Diamond 27 is different than the other diamonds as it has silicic HDF compositions and significant aggregation into B-centres (27% B) in the fibrous growth zones. This implies silicic fluids were active in the mantle significantly before the kimberlite eruption and resulted in an earlier diamond-forming event at Koffiefontein involving both fibrous and monocrystalline diamond growth.
5. Variations in the N−δ^{13}C contents, and fluid inclusions highlight the complexities associated with diamond crystallisation from hydrous carbonate-rich fluids. The processes of crystallisation of fibrous and monocrystalline diamonds may be very similar and the difference in diamond form may simply reflect the degree of carbon supersaturation of the diamond-forming fluid at the point of diamond crystallisation and hence the rate of crystallisation. The presence of monocrystalline rims on relatively young fibrous diamond cores indicates that some monocrystalline diamonds also formed shortly before kimberlite eruption.

Acknowledgements

JWH thanks the Diamond Trading Company (a member of the DeBeers Group of Companies) for the donation of the diamonds used in this study. The authors acknowledge the facilities of the Australian Microscopy & Microanalysis Research Facility at the Centre of Advanced Microscopy, The Australian National University. We thank Hua Chen (SEM), Frank Brink (SEM) and Peter Holden (SHRIMP) for their help with instrument operation. This work was funded by the Australian Research Council (DP140101976) to Masahiko Honda, David Phillips, ALJ and Debra Araujo and supported by AGRTP and Ringwood scholarships to ST. We thank Oded Navon for discussions and helpful comments on an early draft, and an anonymous reviewer, Katie Smart, and editor Klaus Mezger for constructive reviews that significantly improved the presentation of the paper.

References

Bottinga, Y., 1969. Calculated fractionation factors for carbon and hydrogen isotope exchange in the system calcite-carbon dioxide-graphite-methane-hydrogen-water vapor. Geochimica et Cosmochimica Acta, 33(1): 49-64.

Boyd, S. et al., 1987. Multiple growth events during diamond genesis: an integrated study of carbon and nitrogen isotopes and nitrogen aggregation state in coated stones. Earth and Planetary Science Letters, 86(2-4): 341-353.

Boyd, S., Pillinger, C., Milledge, H., Mendelssohn, M., Seal, M., 1992. C and N isotopic composition and the infrared absorption spectra of coated diamonds: evidence for the regional uniformity of CO2H2O rich fluids in lithospheric mantle. Earth and Planetary Science Letters, 109(3-4): 633-644.

Boyd, S.R., Pineau, F., Javoy, M., 1994. Modelling the growth of natural diamonds. Chemical Geology, 116(1-2): 29-42.

Brey, G.P., Bulatov, V.K., Girnis, A.V., Lahaye, Y., 2008. Experimental melting of carbonated peridotite at 6–10 GPa. Journal of Petrology, 49(4): 797-821.

Cartigny, P., Harris, J.W., Javoy, M., 2001. Diamond genesis, mantle fractionations and mantle nitrogen content: a study of δ 13 C–N concentrations in diamonds. Earth and Planetary Science Letters, 185(1): 85-98.

Chacko, T., Cole, D.R., Horita, J., 2001. Equilibrium oxygen, hydrogen and carbon isotope fractionation factors applicable to geologic systems. Reviews in mineralogy and geochemistry, 43(1): 1-81.

Chacko, T., Mayeda, T.K., Clayton, R.N., Goldsmith, J.R., 1991. Oxygen and carbon isotope fractionations between CO2 and calcite. Geochimica et Cosmochimica Acta, 55(10): 2867-2882.

Davis, G., 1978. Zircons from the mantle. . Fourth International Conference on Geochronology, Cosmochronology and Isotope Geology – Abstract: 86-88.

de Vries, D.W. et al., 2013. Micron-scale coupled carbon isotope and nitrogen abundance variations in diamonds: Evidence for episodic diamond formation beneath the Siberian Craton. Geochimica et Cosmochimica Acta, 100: 176-199.

Deines, P., Harris, J., Gurney, J., 1991. The carbon isotopic composition and nitrogen content of lithospheric and asthenospheric diamonds from the Jagersfontein and Koffiefontein kimberlite, South Africa. Geochimica et Cosmochimica Acta, 55(9): 2615-2625.

Farmer, V., 1958. The infrared spectra of talc, saponite and hectorite. Mineral. Mag, 31(241): 829-845.

Goss, J. et al., 2003. Extended defects in diamond: the interstitial platelet. Physical Review B, 67(16): 165208.

Harlow, G.E., 1997. K in clinopyroxene at high pressure and temperature: an experimental study. American Mineralogist, 82(3-4): 259-269.

Harris, J., Gurney, J., 1979. Inclusions in diamond. The properties of diamond: 555-591.

Harte, B., Fitzsimons, I., Harris, J., Otter, M., 1999. Carbon isotope ratios and nitrogen abundances in relation to cathodoluminescence characteristics for some diamonds from the Kaapvaal Province, S. Africa. Mineralogical Magazine, 63(6): 829-829.

Irifune, T., Kurio, A., Sakamoto, S., Inoue, T., Sumiya, H., 2003. Materials: Ultrahard polycrystalline diamond from graphite. Nature, 421(6923): 599.

Izraeli, E.S., Harris, J.W., Navon, O., 2001. Brine inclusions in diamonds: a new upper mantle fluid. Earth and Planetary Science Letters, 187(3): 323-332.

Izraeli, E.S., Harris, J.W., Navon, O., 2004. Fluid and mineral inclusions in cloudy diamonds from Koffiefontein, South Africa. Geochimica et Cosmochimica Acta, 68(11): 2561-2575.

Jablon, B.M., Navon, O., 2016. Most diamonds were created equal. Earth and Planetary Science Letters, 443: 41-47.

Javoy, M., Pineau, F., Iiyama, I., 1978. Experimental determination of the isotopic fractionation between gaseous CO 2 and carbon dissolved in tholeiitic magma. Contributions to Mineralogy and Petrology, 67(1): 35-39.

Kessel, R., Ulmer, P., Pettke, T., Schmidt, M., Thompson, A., 2005. The water–basalt system at 4 to 6 GPa: phase relations and second critical endpoint in a K-free eclogite at 700 to 1400 C. Earth and Planetary Science Letters, 237(3-4): 873-892.

Kessel, R., Ulmer, P., Pettke, T., Schmidt, M.W., Thompson, A.B., 2004. A novel approach to determine high-pressure high-temperature fluid and melt compositions using diamond-trap experiments. American Mineralogist, 89(7): 1078-1086.

Klein-BenDavid, O., Izraeli, E.S., Hauri, E., Navon, O., 2004. Mantle fluid evolution—a tale of one diamond. Lithos, 77(1): 243-253.

Klein-BenDavid, O., Izraeli, E.S., Hauri, E., Navon, O., 2007. Fluid inclusions in diamonds from the Diavik mine, Canada and the evolution of diamond-forming fluids. Geochimica et Cosmochimica Acta, 71(3): 723-744.

Klein-BenDavid, O. et al., 2009. High-Mg carbonatitic microinclusions in some Yakutian diamonds—a new type of diamond-forming fluid. Lithos, 112: 648-659.

Kopylova, M., Navon, O., Dubrovinsky, L., Khachatryan, G., 2010. Carbonatitic mineralogy of natural diamond-forming fluids. Earth and Planetary Science Letters, 291(1): 126-137.

Logvinova, A., Wirth, R., Tomilenko, A., Afanas'ev, V., Sobolev, N., 2011. The phase composition of crystal-fluid nanoinclusions in alluvial diamonds in the northeastern Siberian Platform. Russian Geology and Geophysics, 52(11): 1286-1297.

Logvinova, A.M., Wirth, R., Fedorova, E.N., Sobolev, N.V., 2008. Nanometre-sized mineral and fluid inclusions in cloudy Siberian diamonds: new insights on diamond formation. European Journal of Mineralogy, 20(3): 317-331.

Mendelssohn, M., Milledge, H., 1995. Geologically significant information from routine analysis of the mid-infrared spectra of diamonds. International Geology Review, 37(2): 95-110.

Meyer, H.O., 1987. Inclusions in diamond. Mantle xenoliths.

Navon, O., 1999. Diamond formation in the Earth's mantle, Proceedings of the 7th International Kimberlite Conference. Cape Town: Red Roof Design, pp. 584-604.

Navon, O., Hutcheon, I., Rossman, G., Wasserburg, G., 1988. Mantle-derived fluids in diamond micro-inclusions.

Nestola, F. et al., 2014. Olivine with diamond-imposed morphology included in diamonds. Syngenesis or protogenesis? International Geology Review, 56(13): 1658-1667.

Nimis, P. et al., 2016. First evidence of hydrous silicic fluid films around solid inclusions in gem-quality diamonds. Lithos, 260: 384-389.

Pearson, D., Shirey, S., Harris, J., Carlson, R., 1998. Sulphide inclusions in diamonds from the Koffiefontein kimberlite, S Africa: constraints on diamond ages and mantle Re–Os systematics. Earth and Planetary Science Letters, 160(3): 311-326.

Petts, D., Stachel, T., Stern, R., Hunt, L., Fomradas, G., 2016. Multiple carbon and nitrogen sources associated with the parental mantle fluids of fibrous diamonds from Diavik, Canada, revealed by SIMS microanalysis. Contributions to Mineralogy and Petrology, 171(2): 1-15.

Rapp, R., Timmerman, S., Lowczak, J., Jaques, A., 2017. Metasomatism of Cratonic Lithosphere by Hydrous, Silica-rich, Fluids Derived from Recycled Sediment: Experimental Insights at 5-7 GPa. 11IKC abstract 4640.

Richet, P., Bottinga, Y., Javoy, M., 1977. A review of hydrogen, carbon, nitrogen, oxygen, sulphur, and chlorine stable isotope fractionation among gaseous molecules. Annual Review of Earth and Planetary Sciences, 5(1): 65-110.

Rickard, R., Harris, J., Gurney, J., Cardoso, P., 1989. Mineral inclusions in diamonds from Koffiefontein mine. Kimberlites and related rocks, 2: 1054-1062.

Safonov, O.G., Perchuk, L.L., Litvin, Y.A., 2007. Melting relations in the chloride–carbonate–silicate systems at high-pressure and the model for formation of alkalic diamond–forming liquids in the upper mantle. Earth and Planetary Science Letters, 253(1): 112-128.

Schrauder, M., Navon, O., 1994. Hydrous and carbonatitic mantle fluids in fibrous diamonds from Jwaneng, Botswana. Geochimica et Cosmochimica Acta, 58(2): 761-771.

Shirey, S.B. et al., 2013. Diamonds and the geology of mantle carbon. Reviews in Mineralogy and Geochemistry, 75(1): 355-421.

Shiryaev, A., Izraeli, E., Hauri, E., Zakharchenko, O., Navon, O., 2005. Chemical, optical and isotopic investigation of fibrous diamonds from Brazil. Russ. Geol. Geophys, 46(12): 1185-1201.

Skuzovatov, S.Y., Zedgenizov, D., Shatsky, V., Ragozin, A., Kuper, K., 2011. Composition of cloudy microinclusions in octahedral diamonds from the Internatsional'naya kimberlite pipe (Yakutia). Russian Geology and Geophysics, 52(1): 85-96.

Smart, K.A. et al., 2011. Diamond growth from oxidized carbon sources beneath the Northern Slave Craton, Canada: a δ 13 C–N study of eclogite-hosted diamonds from the Jericho kimberlite. Geochimica et Cosmochimica Acta, 75(20): 6027-6047.

Smit, K.V., Shirey, S.B., Stern, R.A., Steele, A., Wang, W., 2016. Diamond growth from C–H–N–O recycled fluids in the lithosphere: Evidence from CH4 micro-inclusions and δ13C–δ15N–N content in Marange mixed-habit diamonds. Lithos, 265: 68-81.

Smith, B.S., Danchin, R., Harris, J., Stracke, K., 1984. Kimberlites near Orroroo, South Australia. Kimberlites I: kimberlites and related rocks, Elsevier, Amsterdam: 121-142.

Smith, E.M., Kopylova, M.G., Nowell, G.M., Pearson, D.G., Ryder, J., 2012. Archean mantle fluids preserved in fibrous diamonds from Wawa, Superior craton. Geology, 40(12): 1071-1074.

Spandler, C., Yaxley, G., Green, D.H., Rosenthal, A., 2007. Phase relations and melting of anhydrous K-bearing eclogite from 1200 to 1600 C and 3 to 5 GPa. Journal of Petrology, 49(4): 771-795.

Stachel, T., Chacko, T., Luth, R., 2017. Carbon isotope fractionation during diamond growth in depleted peridotite: Counterintuitive insights from modelling water-maximum CHO fluids as multi-component systems. Earth and Planetary Science Letters, 473: 44-51.

Stachel, T., Harris, J., 2008. The origin of cratonic diamonds—constraints from mineral inclusions. Ore Geology Reviews, 34(1): 5-32.

Stachel, T., Harris, J.W., Muehlenbachs, K., 2009. Sources of carbon in inclusion bearing diamonds. Lithos, 112: 625-637.

Stern, R.A., 2014. Methods and reference materials for SIMS diamond C-and N-isotope analysis.

Sverjensky, D.A., Huang, F., 2015. Diamond formation due to a pH drop during fluid–rock interactions. Nature communications, 6.

Tappert, R., Tappert, M.C., 2011. Diamonds in nature: a guide to rough diamonds. Springer Science & Business Media.

Taylor, W.R., Canil, D., Milledge, H.J., 1996. Kinetics of Ib to IaA nitrogen aggregation in diamond. Geochimica et Cosmochimica Acta, 60(23): 4725-4733.

Taylor, W.R., Jaques, A., Ridd, M., 1990. Nitrogen-defect aggregation characteristics of some Australasian diamonds: time temperature constraints on the source regions of pipe and alluvial diamonds. . American Mineralogist, 75: 1290-1310.

Thomassot, E., Cartigny, P., Harris, J., Viljoen, K.F., 2007. Methane-related diamond crystallization in the Earth's mantle: stable isotope evidences from a single diamond-bearing xenolith. Earth and Planetary Science Letters, 257(3): 362-371.

Tomlinson, E., Jones, A., Harris, J., 2006. Co-existing fluid and silicate inclusions in mantle diamond. Earth and Planetary Science Letters, 250(3): 581-595.

Weiss, Y., Griffin, W., Bell, D., Navon, O., 2011. High-Mg carbonatitic melts in diamonds, kimberlites and the sub-continental lithosphere. Earth and Planetary Science Letters, 309(3): 337-347.

Weiss, Y. et al., 2009. A new model for the evolution of diamond-forming fluids: Evidence from microinclusion-bearing diamonds from Kankan, Guinea. Lithos, 112: 660-674.

Weiss, Y., Kiflawi, I., Davies, N., Navon, O., 2014. High-density fluids and the growth of monocrystalline diamonds. Geochimica et Cosmochimica Acta, 141: 145-159.

Weiss, Y., Kiflawi, I., Navon, O., 2010. IR spectroscopy: quantitative determination of the mineralogy and bulk composition of fluid microinclusions in diamonds. Chemical Geology, 275(1): 26-34.

Weiss, Y., McNeill, J., Pearson, D.G., Nowell, G.M., Ottley, C.J., 2015. Highly saline fluids from a subducting slab as the source for fluid-rich diamonds. Nature, 524(7565): 339-342.

Yaxley, G.M., Brey, G.P., 2004. Phase relations of carbonate-bearing eclogite assemblages from 2.5 to 5.5 GPa: implications for petrogenesis of carbonatites. Contributions to Mineralogy and Petrology, 146(5): 606-619.

Zedgenizov, D. et al., 2006. Directional chemical variations in diamonds showing octahedral following cuboid growth. Contributions to Mineralogy and Petrology, 151(1): 45-57.

Zedgenizov, D. et al., 2009. Mg and Fe-rich carbonate–silicate high-density fluids in cuboid diamonds from the Internationalnaya kimberlite pipe (Yakutia). Lithos, 112: 638-647.

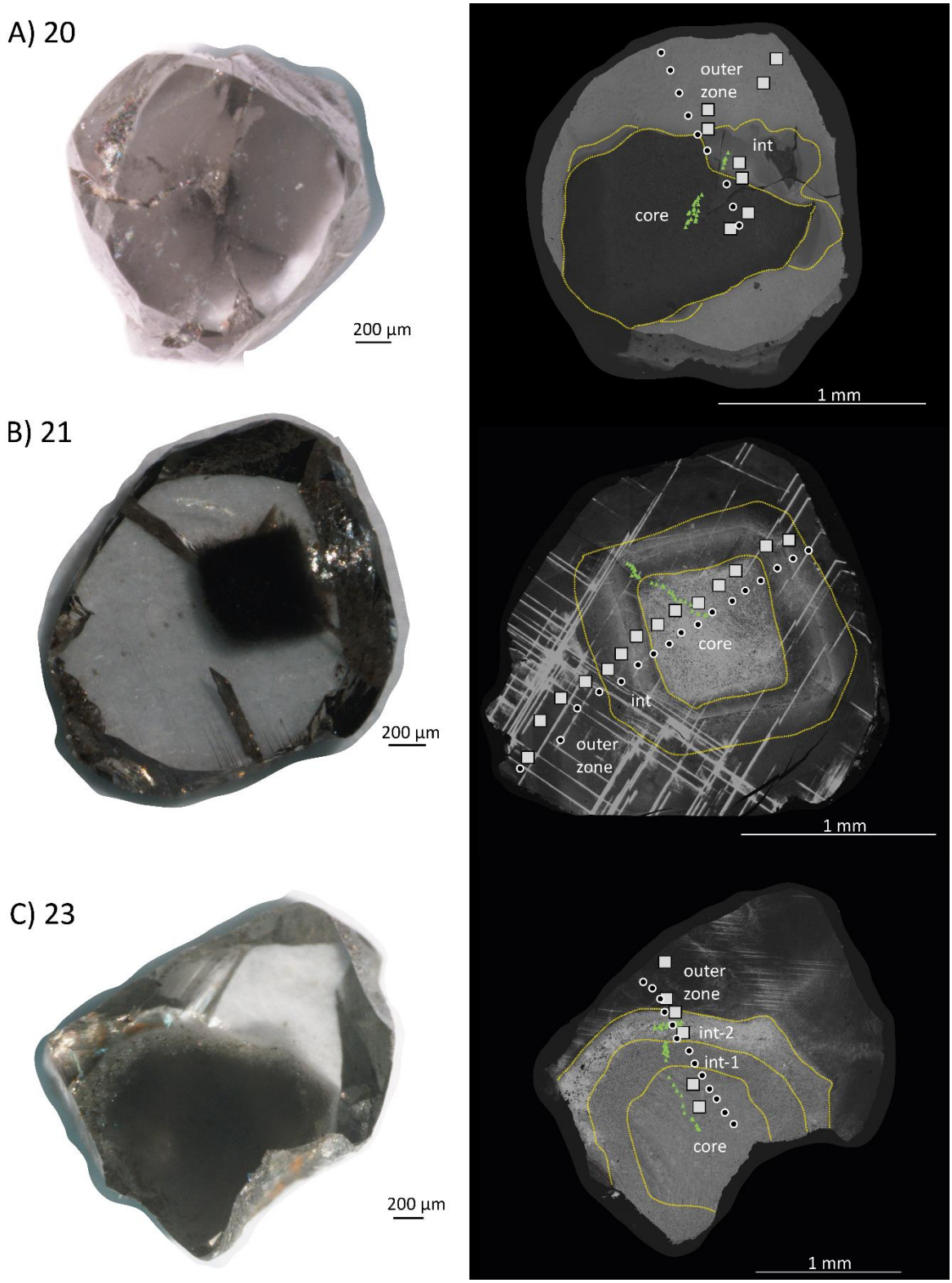

Figure 1: Reflected light and cathodoluminescence images of diamond-20, 21, 23, 27, 28, and 29 from the Koffiefontein mine that were analysed in the present study. Yellow lines represent the interpreted borders between core, intermediate and outer growth zones. The white circles represent the locations of the SHRIMP spot analyses for C isotope compositions, white squares represent the locations of FTIR analyses

for nitrogen, and green triangles the position of SEM-EDS analyses for micro-inclusion major element compositions. Spot sizes were 1 µm for SEM-EDS analyses, 27 µm for SHRIMP analyses, and 100x100 µm for FTIR analyses. For visibility, the symbols have a similar size in the figure.

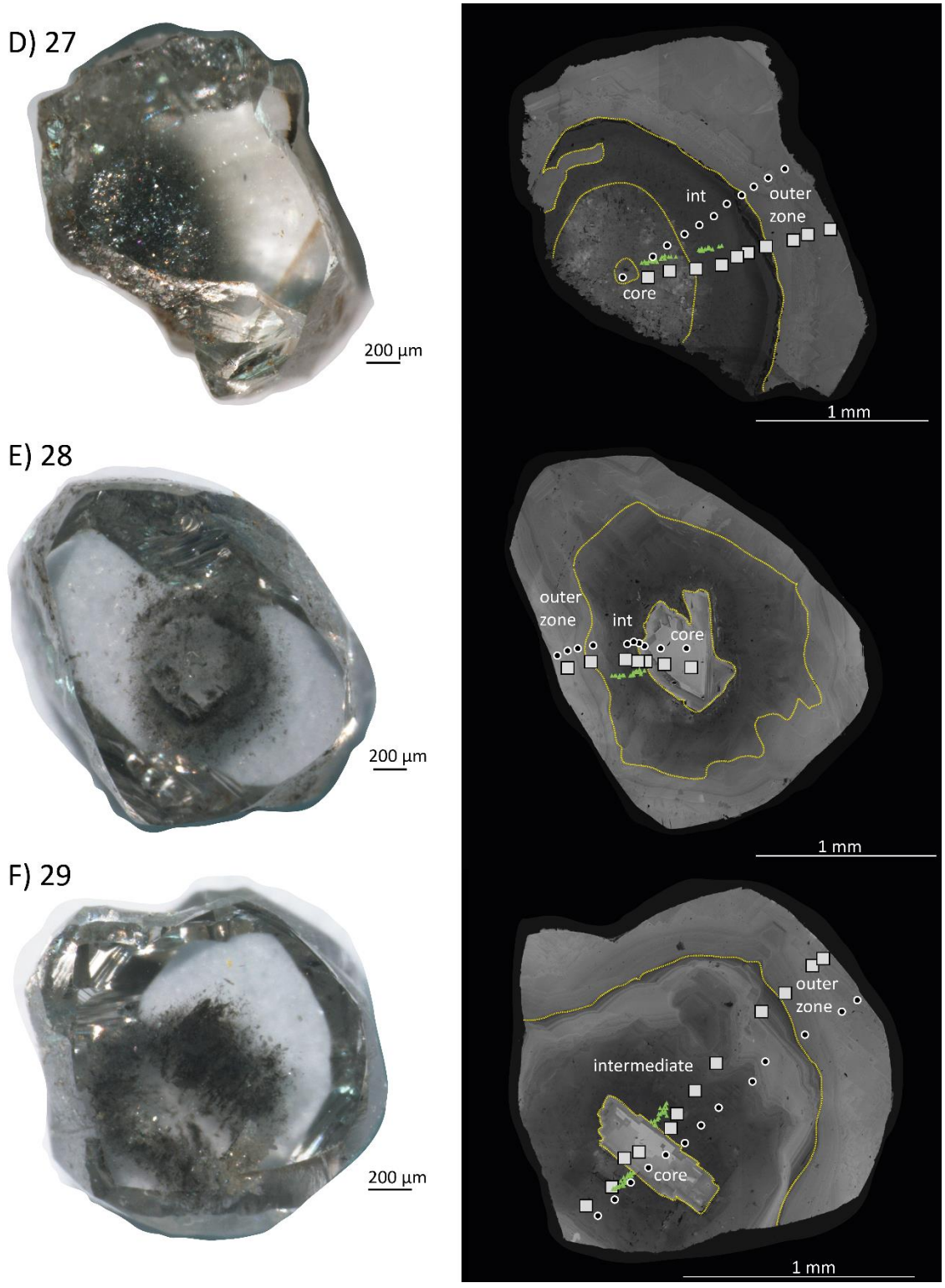

Figure 1 continued

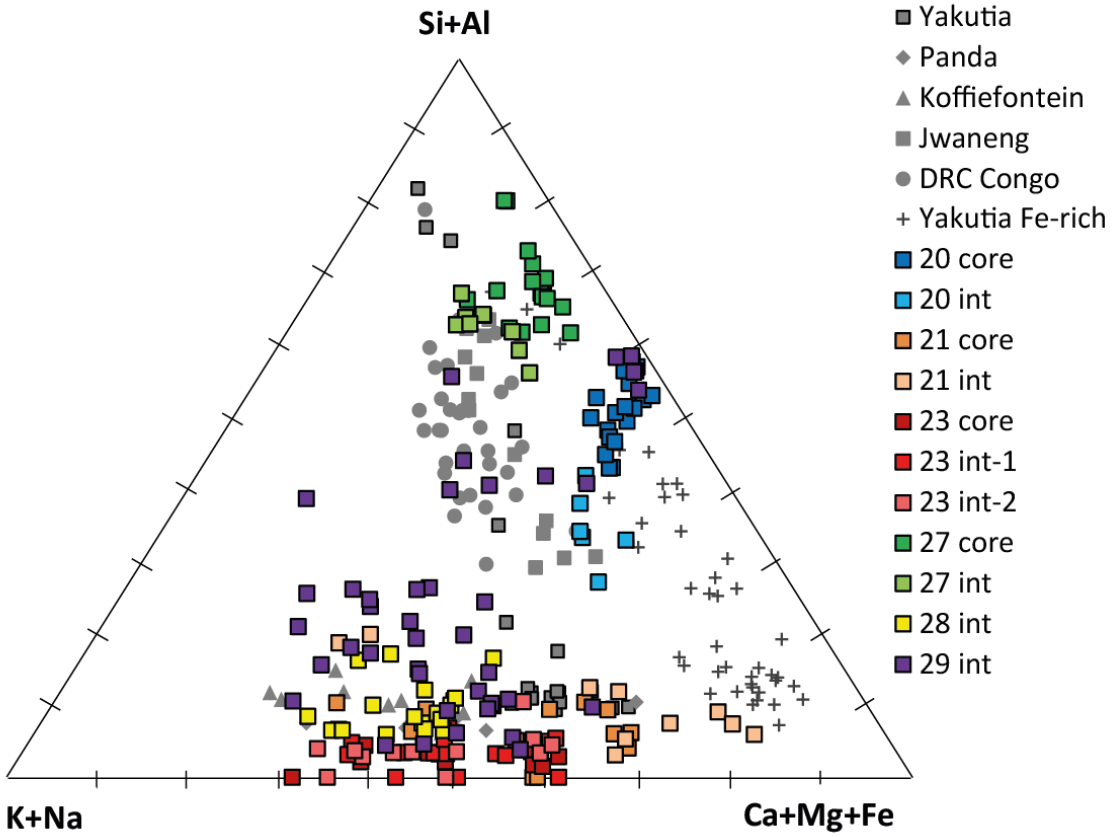

Figure 2: Ternary diagram of silicic, carbonatitic and saline fluid compositions of micro-inclusions in fibrous diamond growth zones. It shows the range of compositions of individual analyses of this study and averages of analyses per diamond from the literature (Izraeli et al., 2001; Klein-BenDavid et al., 2009; Kopylova et al., 2010; Navon et al., 1988; Schrauder and Navon, 1994; Tomlinson et al., 2006; Zedgenizov et al., 2009).

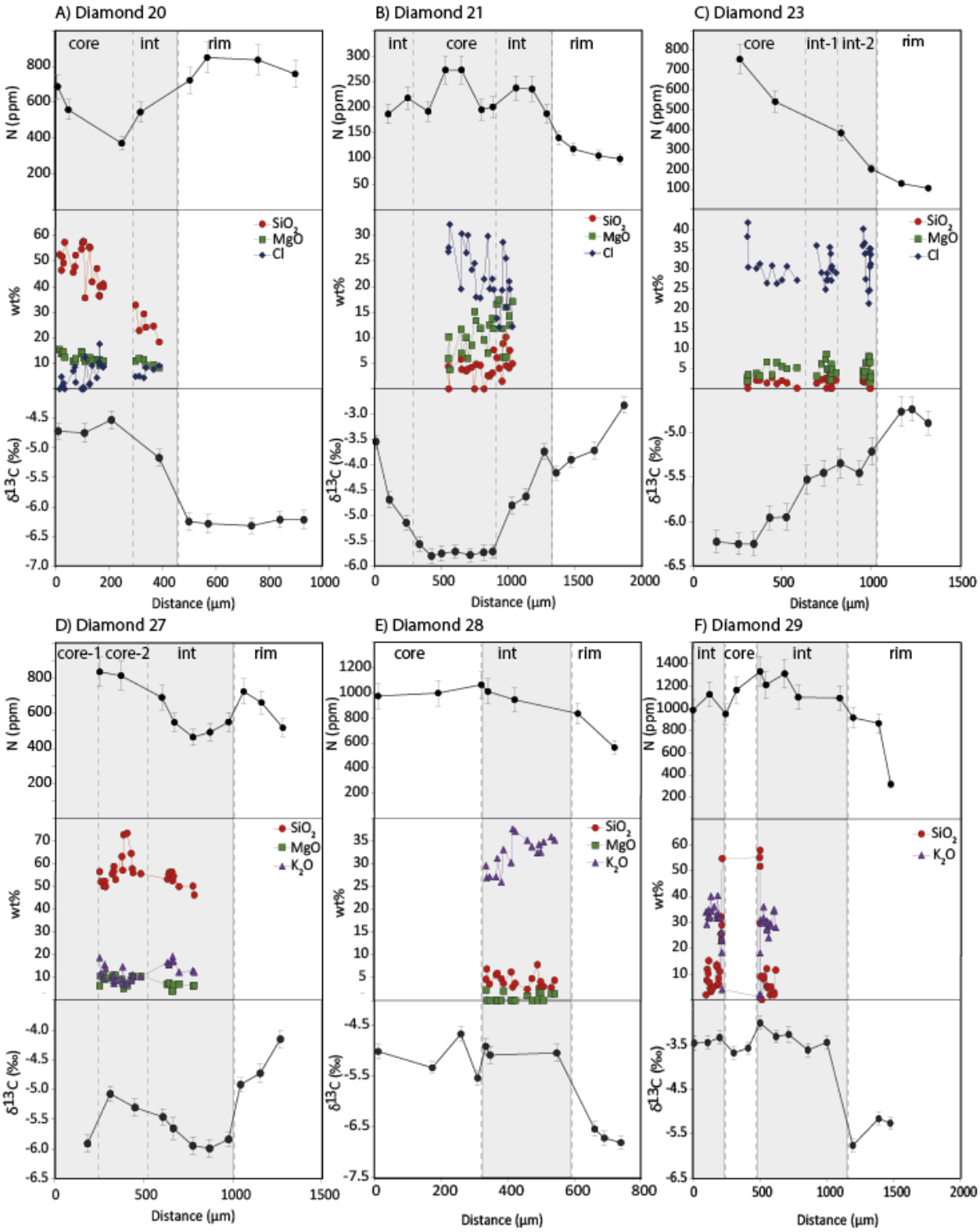

Figure 3: Diagrams showing the change in nitrogen concentration, a selection of major elements and carbon isotope composition, from core to outer zone in the studied diamonds. The grey areas represent the fibrous growth zones, the white areas the monocrystalline growth zones. The change in SiO_2 and MgO is most pronounced and therefore chosen to display the change in major element composition. MgO is not displayed in Fig. 3F due to the overlap of MgO and SiO_2. A) diamond 20, B) diamond 21, C) diamond 23,

D) diamond 27, E) diamond 28, F) diamond 29. For the profiles in figure 3 the carbon isotope analyses profile line was chosen as the reference profile line. The position of each N and inclusion data point was projected onto the C profile line, as can be seen in the supplementary information figure A4. The deviation between the profiles in diamond 20 and 21 are not ideal, but the position in the growth layers was used to make a good projection onto the C profile line.

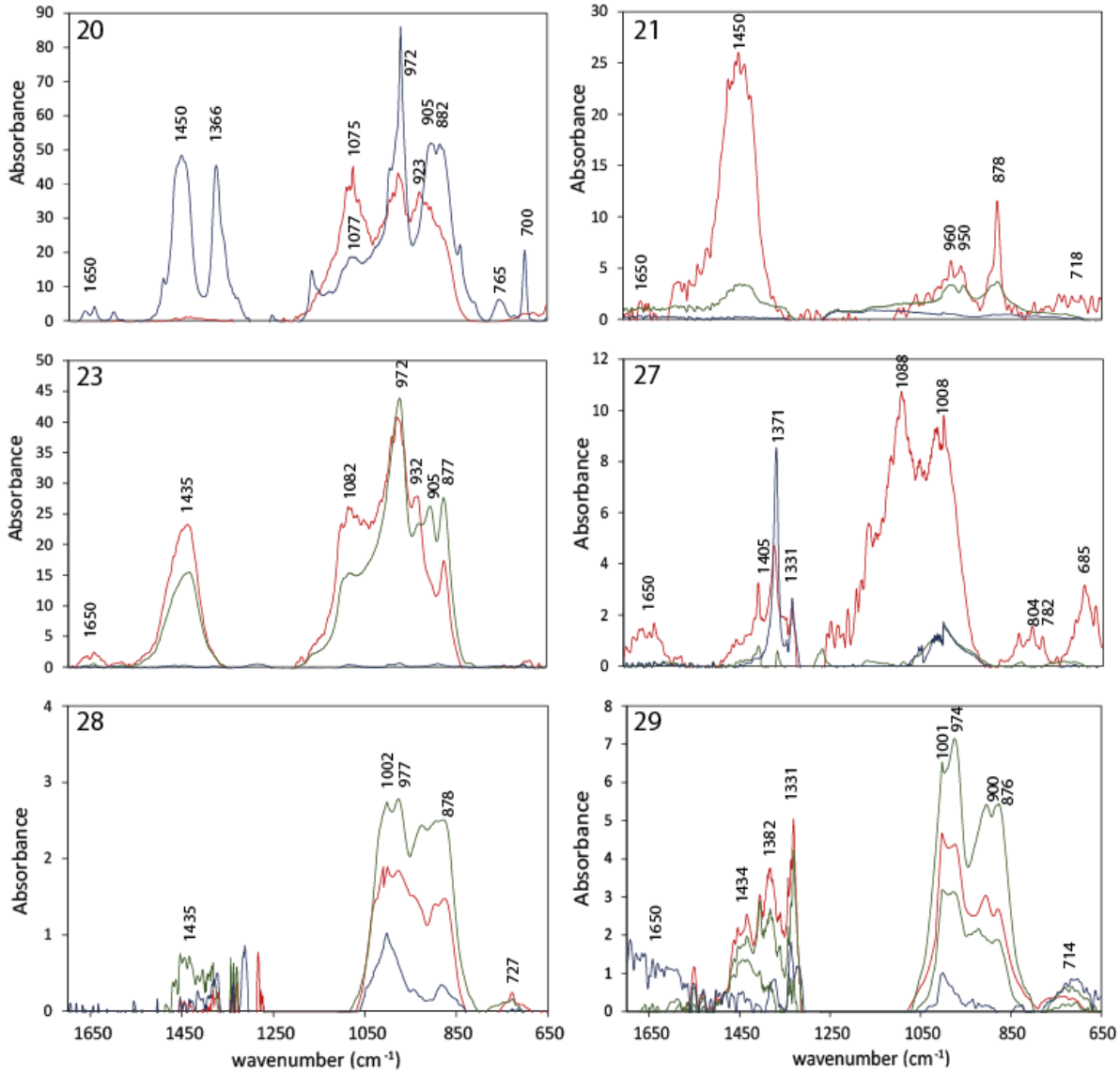

Figure 4: FTIR spectra of the studied diamonds from Koffiefontein, after baseline correction, re-scaling to 1 cm diamond thickness and subtraction of the nitrogen peaks. The cores (red), intermediate (green) and outer zones (blue) correspond to the layers defined in the cathodoluminescence images in Figure 1. Each peak is indicated with the wavenumber of the peak centre and the mineral identification to these peaks is given in section 3.2 Diamond impurities – FTIR spectroscopy.

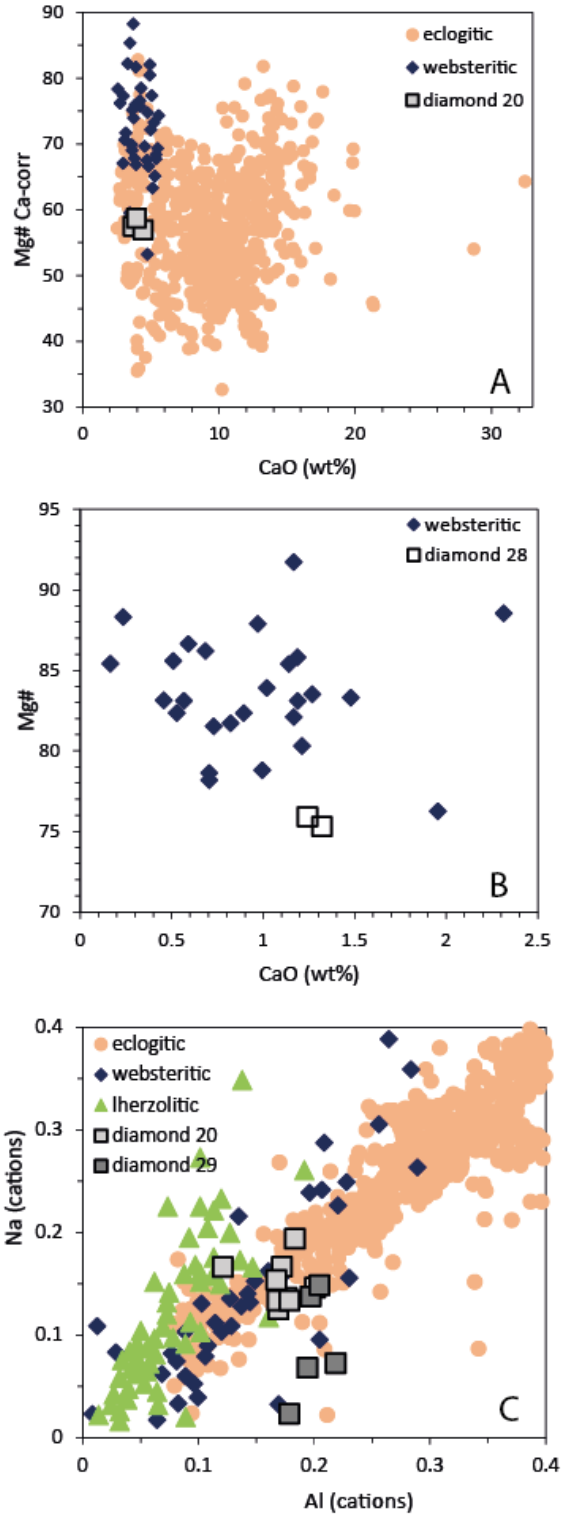

Figure 5: A) Mg# (magnesium number Mg/(Mg+Fe) mole fraction) versus CaO (wt.%) for eclogitic garnet mineral inclusions of diamond 20. B) Mg# versus CaO (wt.%) for websteritic orthopyroxene mineral inclusions of diamond 28. C) Na versus Al in cations per formula unit (6 oxygens basis) for clinopyroxene mineral inclusions of diamond 20 and 29. Reference data are of large mineral inclusions in monocrystalline diamonds (Stachel and Harris, 2008 and references therein).

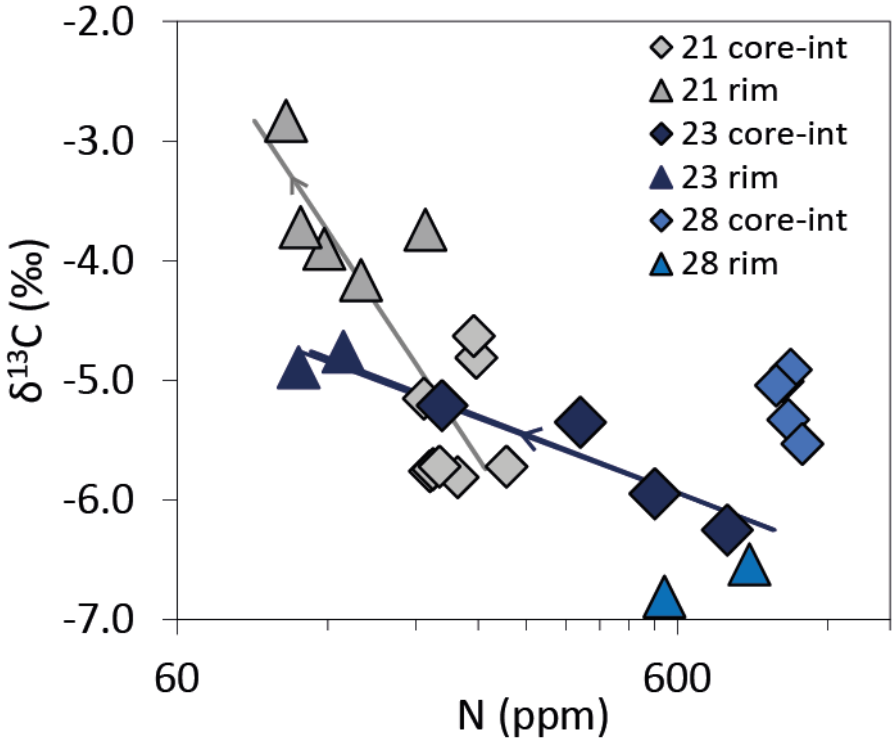

Figure 6: $\delta^{13}C$ versus nitrogen concentration variation, showing the carbon isotope composition is systematically increasing from core to rim while the nitrogen concentration is decreasing for diamond 21 and 23. Symbols represent the data points, the lines are Rayleigh fractionation models, with best fits obtained with a starting $\delta^{13}C_0$ and N content of -6.0‰ and 255 ppm for diamond 21 and -6.1‰ and 940 ppm for diamond 23. The K_N for the Rayleigh fractionation lines are 1.6 and 2.3 for diamond 21 and 3.2 and 6.0 for diamond 23 for CO_3^{2-} and CO_2 respectively. For diamond 28 the core is different than the rim and it appears there is no fractionation trend present.

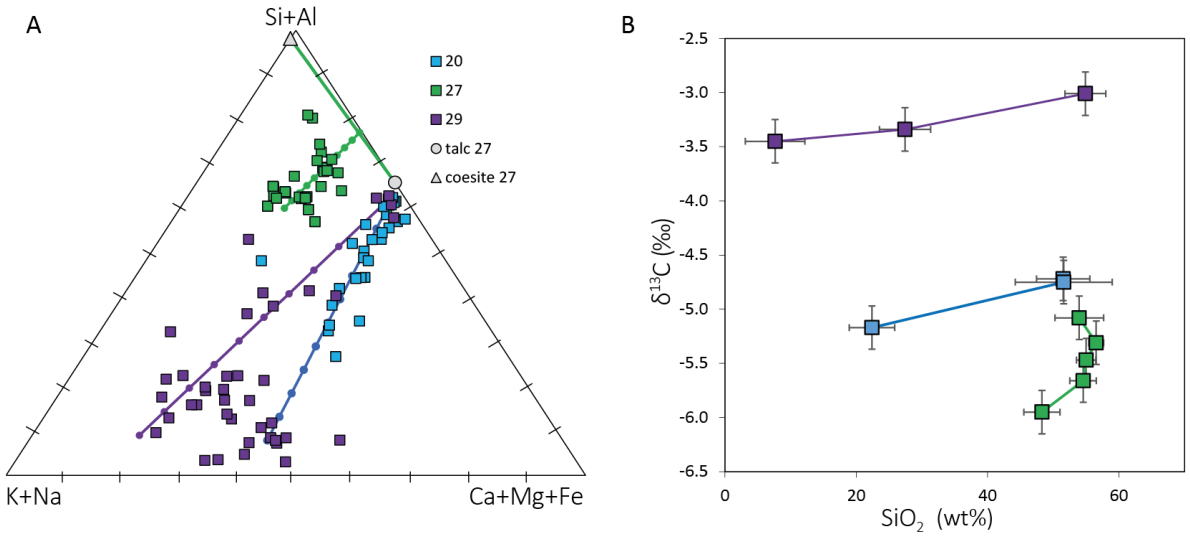

Figure 7: A) A mix between fluids and pyroxene (diamond 20, 29) or talc+quartz (diamond 27). The mixing lines are calculated by using a linear trendline and projecting forwards or backwards to the endmember mineral and fluid compositions. Points on the mixing lines represent the 10% intervals (10% fluid-90% mineral, 20% fluid-80% mineral etcetera). B) The $\delta^{13}C$- SiO_2 compositional change is plotted for samples 20, 27, and 29, based on Table 1 ($\delta^{13}C$) and Supplementary information Table A1 (SiO_2). It shows a decreasing silica content and carbon isotope composition with similar slopes for diamonds 20 and 29 with saline HDFs.

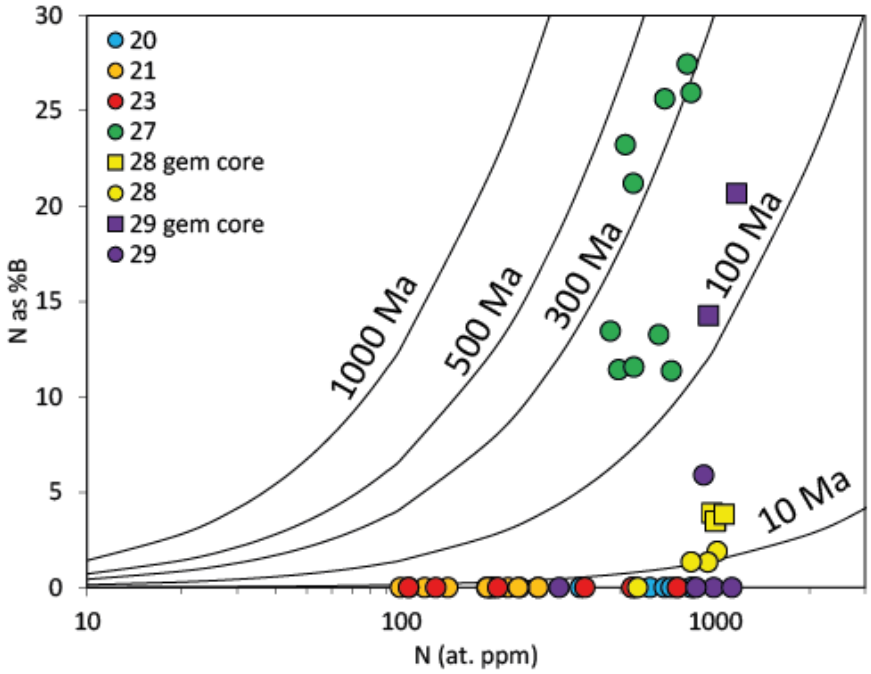

Figure 8: The change in nitrogen aggregation state and concentration of the studied samples, showing the majority of the samples are likely to be young and have short time gaps between growth zones. The exception is diamond 27 with significant B centres present in the fibrous growth zone. The isochrons are calculated with a temperature of 1150°C (based on the average formation temperature at Koffiefontein; 1120±95°C; Izraeli et al., 2004; Rickard et al., 1989) and the parameters of Taylor et al, 1996.

Table 1: Carbon isotope compositions and nitrogen concentrations in the studied Koffiefontein diamonds.

Sample	$\delta^{13}C$ (‰)[a]	N (ppm)[b]	B %	Zone[c]	Sample	$\delta^{13}C$ (‰)	N (ppm)	B %	Zone
20-1	-4.72	687	0	core	27-1	-5.91			core-1
20-2	-4.75	558	0	core	27-2	-5.08	835	26	core-2
20-3	-4.53	371	0	core	27-3	-5.31	814	27	core-2
20-4	-5.17	545	0	int	27-4	-5.47	690	26	int
20-5	-6.25	723	0	outer zone	27-5	-5.66	548	21	int
20-6	-6.28			outer zone	27-6	-5.95	463	13	int
20-7	-6.32	849	0	outer zone	27-7	-6.00	492	11	int
20-8	-6.21	836	0	outer zone	27-8	-5.84	550	12	int
20-9	-6.22	758	0	outer zone	27-9	-4.92	724	11	outer zone
					27-10	-4.73	660	13	outer zone
21-1	-3.55			int	27-11	-4.15	517	23	outer zone
21-2	-4.69	187	0	int					
21-3	-5.15	218	0	int	28-1	-5.01	975	3.9	core-1
21-4	-5.58			core	28-2	-5.33	999	3.5	core-1
21-5	-5.81	192	0	core	28-3	-4.66			core-2
21-6	-5.76	273	0	core	28-4	-5.53	1066	3.8	core-2
21-7	-5.72	273	0	core	28-5	-4.91	1012	1.9	int
21-8	-5.79			core	28-6	-5.08			int
21-9	-5.74	195	0	core	28-7	-5.04	946	1.3	int
21-10	-5.72	201	0	core	28-8	-6.54	836	1.3	outer zone
21-11	-4.81	238	0	int	28-9	-6.72			outer zone
21-12	-4.63	235	0	int	28-10	-6.81	565	0	outer zone
21-13	-3.74	188	0	int					
21-14	-4.16	140	0	outer zone	29-1	-3.46	987	0	int
21-15	-3.90	118	0	outer zone	29-2	-3.45	1128	0	int
21-16	-3.72	106	0	outer zone	29-3	-3.34			int
21-17	-2.83	99	0	outer zone	29-4	-3.68	951	14	core
					29-5	-3.57	1167	21	core
23-1	-6.23			core	29-6	-3.01	1334	19	int
23-2	-6.25	755	0	core	29-7	-3.31	1213	15	int
23-3	-6.25			core	29-8	-3.27	1315	9	int
23-4	-5.96			core	29-9	-3.62	1102	4	int
23-5	-5.95	541	0	core	29-10	-3.45	1096	4	int
23-6	-5.53			int-1	29-11	-5.77	918	6	outer zone
23-7	-5.45			int-1	29-12	-5.16	867	0	outer zone
23-8	-5.35	384	0	int-2	29-13	-5.26	317	0	outer zone
23-9	-5.46			int-2					
23-10	-5.21	203	0	int-2					
23-11	-4.76	129	0	outer zone					
23-12	-4.74			outer zone					
23-13	-4.89	105	0	outer zone					

[a]The error on the $\delta^{13}C$ measurements is 0.27‰ (two standard error) based on repeat analyses of standards MC08 and BS249.

[b]Estimated error for N concentrations is ~10%.

[c]Analyses were performed along core-to-rim cross-sections as indicated in Fig. 1.

The FTIR measurements 29-6 to 29-10 of the intermediate zone of diamond 29 have nitrogen in B centres possibly caused by interference of the core due to the thickness of the plate.

Table 2: Average composition of inclusions in the studied Koffiefontein diamonds

Sample	**20 core**		**20 int**		**21 core**		**21 int**		**23 core**		**23 int-1**	
Description	**Sil-low Mg**		**transitional**		**Carb.**		**Carb.**		**Saline**		**Saline**	
	Ave	**SD**	**Ave**	**SD**	**Ave**	**SD**	**Ave**	**SD**	**Ave**	**SD**	**Ave**	**SD**
Nr. of inclusions analysed	**15**		**6**		**17**		**10**		**12**		**13**	
Na_2O	3.1	1.4	0.9	1	9.3	2	5	2.6	18.3	4.7	15.5	5.2
MgO	11.9	1.3	10.3	1.4	10.2	3.4	13	4.2	4.1	1.6	4.8	1.8
Al_2O_3	4	1.3	5.5	2.2	2.2	2.5	2.3	1	0.5	0.7	0.6	0.8
SiO_2	44.3	8.1	25.4	5.1	3.5	2	5.9	2.6	1.4	1.1	1.5	1
P_2O_5	0.1	0	3	1.7	0.3	1.1	0.5	0.8	0.5	0.9	0.5	0.9
Cl	7.2	5	6.6	2	22.8	6.8	18.8	5.5	31.3	4.8	30	3.3
K_2O	6.6	4.6	21.7	3	27.1	6.3	25.1	9.9	19.5	7.7	22.4	7.7
CaO	14.8	2	10.6	2.3	15.6	5.5	16.2	8	7.7	3	7.3	1.4
TiO_2	0	0	1.4	1.5	0	0	0	0	0.2	0.5	0	0
FeO	8	2.2	14.7	1.8	9	3.8	13.3	7.6	16.5	4.8	17.5	4.8
Total	12.8	5.2	8.3	4	5.3	1.7	9.7	3.4	11.7	1.9	10.3	3
Si+Al	49.3	5.1	34.7	5	6.7	3.7	10.2	5.6	2.7	1.9	3.1	2
Na+K	7.9	3.7	18	2.5	38.5	10.6	29	13.5	51.1	10.5	48.7	8.1
Mg+Ca+Fe	42.8	2.1	47.3	3.8	54.8	10.4	60.8	18.1	46.2	9.9	48.2	8
H_2O/CO_2+H_2O[a]	0.92				0.66		0.67		0.62		0.49	
CO_2 (ppm)	15				398		56		375		255	
H_2O (ppm)	169				777		112		615		248	

[a] Water and carbon dioxide contents were calculated from peak heights at 3420 and 1430 cm^{-1} respectively with the absorption coefficients of Weiss et al. (2010).

Table 2: continued

Sample	23 int-2		27 core-2		27 int		28 int		29 int end	
Description	Saline		Silicic		Silicic		Saline		Saline	
	Ave	SD	Average	SD	Ave	SD	Ave	SD	Ave	SD
Nr. of analyses	14		17		9		19		25	
Na_2O	15.6	4.9	0.7	1	4.6	0.6	4.8	1.4	1.9	2
MgO	4.5	2.2	9.1	1.8	6.2	1.3	0.8	1	0.5	0.9
Al_2O_3	0.6	0.7	10.5	2	7.6	1.2	0.7	1.2	1.4	1.6
SiO_2	2.1	1.5	58.1	6.9	52.8	3.4	4.5	1.5	6.4	3.8
P_2O_5	0.2	0.5	0.5	1	1.9	2	0.1	0.6	0.3	1
Cl	31.8	5.4	0.2	0.3	0.3	0.5	35.1	3.3	37.2	3.4
K_2O	23.7	6.6	10.9	3.2	15.5	2.4	31.8	4.3	32	3.9
CaO	7.2	2.7	1.9	1	5.6	3.5	4.7	1.4	6.6	2.3
TiO_2	0.1	0.5	0.6	0.9	0.1	0.4	0.3	1.2	0.1	0.6
FeO	14.2	3.7	7.6	1.9	5.4	1.1	17.4	4.2	13.5	4.7
Total	13.4	3.5	11.9	5	8.7	5.4	9	2.5	12.5	10
Si+Al	4	2.6	68.3	5.5	62.7	3.2	9.7	3.5	14.7	7.5
Na+K	52.3	10.2	8.1	3.2	15.6	1.9	49.7	7	46.2	7.7
Mg+Ca+Fe	43.8	9.2	23.5	4.6	21.7	4.4	40.6	6.9	39.2	10.9
H_2O/CO_2+H_2O			0.90		0.87		0.90		0.85	
CO_2 (ppm)			20		4		11		22	
H_2O (ppm)			187		28		99		123	

Table 3: Composition of mineral inclusions in the studied Koffiefontein diamonds.

Sample	Description	SiO_2	Al_2O_3	FeO	MgO	CaO	Na_2O	K_2O	P_2O_5	Cl	Total	O =	Total	Mg#
20 core	calcite	3.17	0.00	0.00	5.53	91.30	0.00	0.00	0.00	0.00	9 .99	3	2.92	
20 core	omph/aug[c]	55.37	4.29	6.89	13.95	16.73	2.76	0.00	0.00	0.00	10.80	6	4.00	78.3
20 core	omph/aug	60.43	4.06	3.97	11.90	17.81	1.83	0.00	0.00	0.00	35.06	6	3.84	84.2
20 core	omph/aug	57.42	4.16	5.61	12.45	18.40	1.96	0.00	0.00	0.00	3.86	6	3.92	79.8
20 core	omph/aug	54.77	2.81	7.26	14.72	18.09	2.35	0.00	0.00	0.00	14.97	6	4.02	78.3
20 core	omph/aug	57.24	4.07	5.62	13.87	16.79	2.40	0.00	0.00	0.00	19.49	6	3.95	81.5
20 core	omph/aug	58.50	3.99	4.68	12.41	18.06	1.93	0.43	0.00	0.00	7.72	6	3.89	82.5
20 core	omph/aug	57.65	4.76	5.17	12.22	18.10	2.11	0.00	0.00	0.00	7.69	6	3.91	80.8
20 core	omph/aug	57.50	4.22	5.67	12.35	18.34	1.92	0.00	0.00	0.00	2.71	6	3.91	79.5
20 core	omph/aug	57.82	3.95	5.73	12.80	17.21	2.21	0.27	0.00	0.00	4.47	6	3.92	79.9
20 int	pyrope-almandine	41.84	21.36	17.07	12.34	3.69	0.00	1.76	0.00	1.94	6.89	12	7.98	56.3
20 int	garnet	40.27	22.01	17.33	12.13	4.41	0.00	1.86	0.00	1.99	6.87	12	8.04	55.5
20 int	garnet	43.21	21.82	16.09	12.21	3.93	0.00	1.72	0.00	1.01	9.97	12	7.93	57.5
21 int	Mg,Ca,Fe CO_3	0.00	0.00	19.08	29.68	43.06	0.00	3.70	1.56	2.91	10.58	3	3.07	
21 int	Mg,Ca,Fe CO_3	8.03	3.93	23.75	29.77	32.08	0.00	2.44	0.00	0.00	5.36	3	2.79	
27 core-2	coesite	90.74	4.34	0.00	0.00	0.00	0.00	1.61	3.31	0.00	9.22	2	1.03	
27 core-2	coesite	93.86	4.27	0.00	0.00	0.00	0.00	1.87	0.00	0.00	7.77	2	1.03	
27 core-2	talc	64.38	1.39	5.95	28.28	0.00	0.00	0.00	0.00	0.00	12.71	10	6.34	89.4
27 int	calcite	0.00	6.29	0.00	0.00	93.71	0.00	0.00	0.00	0.00	7.12	3	2.90	
28 int	enstatite-ferrosilite	53.41	1.21	15.95	28.18	1.24	0.00	0.00	0.00	0.00	23.65	6	4.04	75.9
28 int	enstatite-ferrosilite	52.65	1.57	16.25	27.86	1.32	0.00	0.00	0.00	0.35	23.38	6	4.05	75.3
29 int	diopside	56.70	4.58	4.81	12.50	20.50	0.98	0.00	0.00	0.00	12.60	6	3.85	82.2
29 int	diopside	55.90	5.15	4.91	12.60	20.40	1.04	0.00	0.00	0.00	12.00	6	3.86	82.0
29 int	diopside	56.45	4.62	4.15	12.16	19.96	1.97	0.00	0.00	0.70	2.71	6	3.90	83.9
29 int	diopside	58.25	4.17	3.69	11.98	18.76	0.33	1.88	0.53	0.00	1.85	6	3.81	85.2
29 int	diopside	53.92	4.72	5.57	12.19	20.70	2.09	0.00	0.00	0.81	3.28	6	3.95	79.6

[a]Analyses are expressed in wt%.

[b]Total cations are per formula unit based on the amount of oxygen (O) stated.

[c]The clinopyroxenes of diamond 20 are on the boundary of omphacite and Ca-Mg-Fe pyroxenes. In the nomenclature of Ca-Mg-Fe pyroxenes it would fall into the augite pyroxene field.